Evidence of Silencing of Intestinal Inflammatory and Immune Transcripts Following Induction of Joint Inflammation

Meghan M. Moran[1], Jun Li[2], Quan Shen[3], Anthony Day[4] , Ankur Naqib[1,5], Stefan J. Green[5], D. R. Sumner[1], Anna Plaas[2]

1- Dept. of Anatomy & Cell Biology, Rush University Medical Center (RUMC), Chicago, IL, USA; 2- Dept. Int. Medicine (Rheumatology), RUMC; 3- Dept. of Neurosurgery, RUMC; 4- Dept. of Biology, Medicine and Health, The University of Manchester, UK; 5- Bioinformatics Core, RUMC; 5- Genomics and Microbiome Core Facility, RUMC

ABSTRACT

Disrupted intestinal epithelial barrier function has been proposed to be integral to rheumatoid arthritis (RA) progression and pathogenesis. To further define the molecular pathways in synovial inflammation and a response of the intestinal tissues, we have now used a rat model of mono-joint inflammatory arthritis, induced by intra-articular injection (IAI) of Complete Freund's adjuvant (CFA). The predominant inflammatory response of a single injection of the adjuvant into the knee joint resulted in rapid and reproducible formation of a fibrotic myeloid-infiltrated synovial pannus. Our aim was to determine how intestinal tissues, including the proximal and distal ileum and distal colon, respond to inflammatory changes in the synovium in a temporally coordinated manner by comparing their transcriptomic landscapes using RNASeq analyses. We confirmed the timeline of joint inflammation by knee joint swelling measurement, synovial fluid levels of the acute phase protein Inter-α-trypsin inhibitor heavy chains (ITIH) and demonstrated a self-correcting response of trabecular and cortical bone to the CFA challenge. Intestine-specific responses were monitored by 16S microbiome amplicon sequencing, histopathology for mucus layer integrity, and immune cell immunohistochemistry. We present data showing that the intestinal tissue response to the acute joint inflammation was region specific, with the ileum primarily responding with increased mucus secretion and silencing of T cell specific pathways, whereas the colon showed a transient upregulation of macrophages, with a broader suppression of immune related and metabolic pathway related transcripts. However, at no time after CFA-IAI were there significant changes in the fecal microbiome composition of the ileum or the colon. In summary, our data report for the first time a suppression of intestinal inflammatory and immune responses following the induction of joint inflammation and only minimal and transient changes in the microbiome.

INTRODUCTION

In the past decade, numerous studies have focused on the role of 'gut health' in bone metabolism[1-5]. Gut-bone axis research has also explored the progression of several chronic musculoskeletal disorders and challenges, including rheumatoid arthritis, spondylarthritis, ankylosing spondylitis, psoriatic arthritis[6; 7], osteoarthritis[8] and implant loosening[5]. Other chronic diseases, especially those affecting metabolic homeostasis such as obesity and diabetes[9; 10], cardiovascular disease[11], and neurodegenerative diseases[12] have also been reported to affect and be affected by intestinal functions. Gut-organ axis research has largely focused to date on studying alterations in the composition of the gut microbiota, defined as "dysbiosis", which includes decreased microbial diversity and/or expansion of specific bacterial taxa that affect the host physiology[13].

Acute and chronic inflammatory disease states are accompanied by autocrine and paracrine production of mediators (cytokines, chemokines, and growth factors), activation of immune cells, and modification of enteric neuronal signals. Singly, or in combination, these influences can transform the intestinal environment by altering the microbial profile, mucoid surfaces, and nutrient absorption[14]. Furthermore, environment conditions, such as diet[15], therapeutics[16], or environmental stressors[17] can further perturb the intestinal microenvironment. Since such alterations vary amongst different diseases, disease stages and severity, a broad spectrum of dysbiosis 'signatures' have been reported in the literature[18]. Dysbiosis can be accompanied by a disrupted intestinal barrier, which can allow for the translocation of microbial toxins and microorganism from the intestinal lumen into the circulation, triggering systemic immune stimulation and promoting extra-intestinal diseased organ inflammation and disfunction[10].

The intestinal barrier is composed of an outer mucus layer with the commensal gut microbiota, antimicrobial proteins, secreted immunoglobulin A molecules, a specialized epithelial cell layer, and an inner lamina propria that is populated with innate and adaptive immune cells, including B cells, macrophages, and dendritic cells. This barrier is highly dynamic and responsive to both internal and exogenous stimuli, such as growth factors, cytokines, xenobiotics, bacteria, and diet[19]. A critically important component of this physical barrier is the multicellular intestinal epithelium. It is constantly regenerating, with self-renewing pluripotent stem cells located in crypts that can differentiate into absorptive enterocytes, mucin secreting goblet cells, enteroendocrine cells, Paneth cells, and microfold cells[19]. Furthermore, specific interactions of structural molecules secreted by the epithelial cells such as mucins[20] and tight junction proteins provide limited permeability for nutrient absorption, while also providing a blockade as primary defense against bacteria and immune homeostasis[21].

Disrupted intestinal epithelial barrier function has been proposed to be integral to rheumatoid arthritis (RA) progression and pathogenesis[22; 23]. In fact, an early disease response in an RA murine model has been shown to be through Zonulin-CXCR3 mediated dissociation of tight junctions[24]. Furthermore, elevated HIF2α in intestinal epithelial cells has been shown to accelerate arthritis and its inhibition results in improved intestinal barrier function as well as diminished activation of intestinal and lymphatic T-helper 1 (Th1) and Th17[25]. HIF1α is highly upregulated in intestinal epithelial cells at the onset of arthritis in the same RA murine model and has

been shown to provide protection against necroptosis, intestinal inflammation, and arthritis progression through its repression of the transcriptional factor RIPK3[26; 27].

The mucus layer in the small intestine, a key component of the intestinal barrier, accumulates antibacterial molecules such as defensins and lysozymes, which are produced by Paneth cells in the crypts[28; 29]. Furthermore, IgA stored in the small intestinal mucus, when bound to bacteria, can cause aggregation, leading to slower diffusion and reduced bacterial mobility within the barrier layers. As a result, bacteria are largely excluded from interaction with the epithelium and the Peyer's patches. In the colon, an inner mucus layer also shields the host epithelium from the commensal bacteria and an outer mucus layer provides growth niches and nutrients for commensal bacteria. Alterations to mucin glycosylation patterns occur because of intestinal infection and inflammation and have been implicated in microbiota dysbiosis[30]. For example, terminal sialylation of oligosaccharide structures by the goblet cell sialyltransferase ST6GALNAC1 (ST6), is essential for mucus integrity and protects against excessive bacterial proteolytic degradation. Loss-of function mutations in this sialylation gene causes defective mucus proteins and congenital inflammatory bowel disease (IBD)[31]. Although there are currently no reports on defective intestinal mucin glycosylation in RA, metabolic changes such as those affecting the glycolytic pathway[32] have been reported in RA disease progression[33] and could potentially affect post-translational modification of intestinal mucins.

Under healthy condition, the gut contains innate lymphocytes in the epithelial layer of the intestinal mucosa and the lamina propria[34]. These local cells are important for maintaining or restoring intestinal function within the complex immune environment of the gut, especially in inflammatory disorders. Amongst them are Th17 and regulatory T (Treg) cells, which can differentiate from the innate pool of CD4+ T cells. A Th17/Treg cell ratio is a critical marker in tissue inflammation and autoimmunity suppression as an imbalance will result in intestinal diseases such as autoimmune IBD[35]. Innate lymphoid cells (ILC) also play an important role in intestinal barrier homeostasis[36] contributing to tissue protection, regeneration, and mucosal integrity by eliciting a rapid response to signals or cytokines produced by other cells[37].

In a model of implant loosening, we found that intra-articular administration of cobalt-chromium particles induced synovial tissue inflammation and fibrosis and peri-implant bone loss as well as gut microbial dysbiosis[5]. To further define the molecular pathways in synovial inflammation and a response of the intestinal tissues, we have now used a rat model of mono-joint inflammatory arthritis, induced by intra-articular injection (IAI) of Complete Freund's adjuvant (CFA)[38; 39]. The predominant inflammatory response of a single injection of the adjuvant into the knee joint is the rapid and reproducible formation of a hyperplastic and fibrotic synovial pannus[40]. The synovium is a key inflammatory component in degenerative joint disease[41-43]. In a healthy joint, the synovium is composed of various cell types including fibroblast-like, macrophage-like synoviocytes organized into two layers. The fibroblast-like cells secrete the main components of the synovial fluid and the vasculature found in the synovium provides essential nutrition to the avascular articular cartilage. Macrophage-like cells phagocytose injury-related debris and possible infected tissues present in the joint. The failure of synovial cells to fulfill their functions results in the joint inflammation that is characteristic of RA, OA and psoriatic arthritis[41; 43].

Hyperplasia and vascularization of the synovium brings in immune cells, including B cells, T cells and proinflammatory macrophages leading to pannus formation. Pannus-produced products then promote cartilage matrix damage and continued joint deterioration[41-43].

In addition, the CFA model, when performed in rodents has been reported to produce changes in the intestinal microbiome[44-46]. Here, our aim was to determine how intestinal tissues, including the proximal and distal ileum and distal colon, respond to inflammatory changes in the synovium in a temporally coordinated manner by comparing their transcriptomic landscapes using RNASeq analyses. In addition, we confirmed the timeline of joint inflammation by knee joint swelling measurement, synovial fluid levels of the acute phase protein Inter-α-trypsin inhibitor heavy chains (ITIH) and demonstrated a self-correcting response of trabecular and cortical bone to the CFA challenge. Intestine-specific responses were also monitored by 16S microbiome amplicon sequencing, histopathology for mucus layer integrity, and immune cell immunohistochemistry. We present data showing that the intestinal tissue response to the acute joint inflammation was region specific, with the ileum primarily responding with increased mucus secretion and silencing of T cell specific pathways, whereas the colon showed a transient upregulation of macrophages (CYP3a), with a broader suppression of immune related and metabolic pathway related transcripts. However, at no time after CFA injection were there significant changes in the fecal microbiome composition of the ileum or the colon. In summary, our data report for the first time a detailed examination of changes in all components of the intestinal barrier in response to a local inflammatory response in an articular joint.

Methods

Animal Husbandry. All procedures used in this study were approved and in compliance with the Institutional Animal Care and Use Committee (IACUC) at Rush University Medical Center. A total of 44 male Sprague Dawley (SD) rats (375-400g, approximately 4 months old, Envigo) were pair-housed in cages (polysulfone,19 × 10.5 × 8 in.) in the animal facility maintained at 22°C and 35%-55% humidity with a 12-hour light/dark cycle (light 7 AM-7 PM). Standard laboratory-grade rodent chow (Teklad Global Rodent Diet 2018, 18% protein; Envigo) and water were provided *ad libitum* (**Fig. S1**).

Induction of Knee Joint Inflammation with Complete Freund's Adjuvant. Experiments were initiated after a 2-week acclimatization period to minimize effects of stress conditions during transport and housing, severity, and inter-group inconsistency in disease responses. Intra-articular injections (IAI), blood collections and sacrifice were all conducted at the same time of day, i.e. between 9AM-noon. Rats were assigned to one of three study groups (n=6 rats/group): Naïve (no intra-articular injection), Complete Freund's Adjuvant (CFA, 10mg Mycobacterium tuberculosis, 1.5ml Mannide monooleate and 8.5ml paraffin oil, InvivoGen) and Sham controls (1xPBS). IAI was administered using a 29G insulin syringe lateral to the patellar tendon as a single 50µl dose bilaterally, into the left and right knee joints. At day 0 (day before IAI) and at days 3, 7 and 14 post-IAI, under 3% isoflurane anesthesia, rats were weighed and knee and ankle diameters measured using calipers in the medial-

lateral orientation. Non-fasted tail-vein blood was collected into a BD Vacutainer SST tube per rat. Blood was allowed to clot at room temperature. Serum was separated by centrifugation at 3,000 rpm for 18 min at 4°C (~250 µL per bleed) and 40 µL 10X proteinase inhibitor (PI) cocktail (Sigma Aldrich Fine Chemicals Biosciences cOmplete, Mini, EDTA-free Protease Inhibitor Cocktail, 11836170001) was added prior to storage at -80°C.

Sacrifice, Tissue Collections and Storage. All rats were euthanized by CO_2 inhalation. At sacrifice, synovial fluid was collected by opening the joint capsule while the knee was carefully flexed. The synovial fluid from the right and left knee joints was combined from each individual rat. The joint cavity was rinsed twice with 150µL 1xPBS and collected into sterile microcentrifuge tubes. Lavages were centrifuged at 3,000 rpm for 10 min at 4°C to remove cells and debris. Supernatants were stored at -80ºC until further analyses. Synovial tissue was collected from the peri-meniscal/peri-femoral regions, combined with the dissected patellar fat pad into RNALater and stored at -80ºC for RNA-Seq analyses. Bilateral hindlimbs were collected from all rat and disarticulated at the hip. Left intact knee joints were fixed in 10% neutral-buffered formalin (NBF) and decalcified in 20% EDTA for histology. Intact joints were isolated by making transverse cuts 1.5cm proximal and distal to the joint. The femoral and tibial epiphyses were paraffin processed, embedded and 20 sagittal sections cut from both medial and lateral compartments. Right intact knee joints were dissected open using a fresh scalpel. The synovium and patellar fat pad were excised and placed into a 1.5 mL microcentrifuge tube containing 1 mL RNALater (Invitrogen, Thermo Fisher, AM7021) and frozen at -80°C until RNA extraction.

Ileum and colon were dissected and fecal contents expressed into sterile 1.5ml microcentrifuge tubes from both gut segments and were stored at -80ºC for 16S microbiome analyses. Ileum and colon tissues were dissected and either rinsed twice with ice-cold 1 x PBS, transferred to RNALater on ice and stored at -80ºC for RNASeq or placed into Modified Bouin's fixative and prepared into Swiss rolls[47; 48] post-fixed in 10% NBF for paraffin embedding. Forty 6 µm thickness sections were cut from the mid portion of the Swiss roll (**Fig. S1**).

Histopathology of Intestinal Tissues. Paraffin sections from the mid-regions of the Swiss rolls underwent Hematoxylin & Eosin (H&E) staining (Harris Hematoxylin, Electron Microscopy Science, 26754-01; Eosin, Sigma HT110116) for standard pathology evaluation. Alcian Blue (Vector Labs, Alcian Blue (pH 2.5) Stain Kit, H-3501) was completed on consecutive sections for identification of goblet cells and mucus layers. Histopathology for three biotinylated mucin O-linked specific lectins: Griffonia (Bandeiraea) Simplidifolia Lectin I (GSL I, Vector Labs, B-1105-2); Maackia Amurensis Lectin II (MAL II, Vector Labs, B-1265-1) and Ulex Europaeus Agglutinin I (UEA I, Vector Labs, B-1065-2) were also completed on adjacent sections.

Quantitative Western Blot Analyses of serum and synovial fluid bikunin. Control mouse serum was treated the same as experimental rat serum and included in each western blot as an internal standard. Serum samples were thawed on ice and diluted 1:1 with 50mM ammonium acetate pH 7.0 containing 1X PI and debris removed with

a 0.45 µM filters. 150µL of sera were desalted using MicroCon 3 filtration units (at 12,500 rpm for 15 min) and retentates washed once with 450µL 50mM ammonium acetate, pH 7. Desalted proteins were collected from the membrane with 500µL ammonium acetate, pH 7.0. Portions (containing 7.5µL equivalents of serum) were incubated at 37°C for 2 hrs with or without 5 mU of protease-free chondroitinase ABC (Chondroitinase ABC protease free, AMS.E1028-02).

Synovial fluid samples were thawed on ice, diluted to 450µL with 50 mM ammonium acetate, pH 7 containing PI, clarified by centrifugation at 12,000 rpm at 4 C for 15 min, and desalted using MicroCon 3 filtration units as described above for serum samples. The retentate was recovered in 200µL 50 mM ammonium acetate, pH 7 and 100µL portions were incubated at 37°C for 2h with or without 5 mU of protease-free chondroitinase ABC.

Sera and synovial fluid samples were speedvac dried and analyzed by gel electrophoresis and western blot. Chondroitinase digestion buffer was removed by speedvac evaporation, and samples dissolved in Tris-glycine SDS sample buffer (Novex, AMS.E1028-02) containing 100µl of 0.5M DTT, heated at 90°C for 5 min before electrophoresis on 10% SDS gels (Invitrogen Novex WedgeWell 10% Tris-Glycine, XP00102Box). Separated proteins were electro-transferred on ice (250V, 302µA for 45 min and 150V, 297µA for 15 min) to 0.45µm nitrocellulose membranes (BioRad, 1620115). Western blotting of membranes with anti-bikunin (MIM126, ap_A_mBikunin, AVLPQESEGSC-NH_2; or CP6, ap_B_hBikunin, AVLPQEEEGSC-NH_2) was completed as previously published[49] and chemiluminescent images taken using an iBright1500 (Invitrogen, Thermo Fisher). Images were analyzed using ImageJ software[50] and data expressed as incident power density (IPD) relative to standard mouse serum.

Micro-computed Tomography analyses of femurs. MicroCT scanning was completed using a Scanco µCT50 (Switzerland). Right femurs were scanned using 70 kVp, 114 µA, and 10µm voxel size. The region of interest (ROI) for trabecular and cortical bone analyses started just proximal to the distal femoral growth plate and continued 2 mm proximally into the metaphysis. The trabecular and cortical bone compartments were analyzed separately using thresholds of 200 and 1000, respectively. Periosteal reaction was noted when present and analyzed separately from the cortex using the same threshold values.

RNASeq Analyses of Synovium and Intestine. To obtain reproducible and high-quality yields of RNA from synovium, tissues were harvested from right and left knees and pooled from n=3 rats, then analyzed as a single sample. Distal ileum and colon tissues in RNAlater were thawed on ice and 1 cm pieces were dissected out (including villi, submucosa, and smooth muscle layers) using transverse cuts. Using previously published methods[51],all tissues underwent extraction and purification of RNA. Samples with RIN numbers $\geq$7 were reverse transcribed into cDNA, PCR amplified with primers CS1_515F and CS2_806R, and a library was prepared.

Bioinformatic analyses of sequencing data was carried out as follows: Raw reads were trimmed to remove Truseq adapters and bases from the 3' end with quality scores less than 20 using cutadapt[52]; trimmed reads shorter than 40bp were discarded, and were then aligned to the mRatBN7.2 *Rattus norvegicus* (Norway rat) reference genome using STAR[53]. The expression level of ENSEMBL genes was quantified using FeatureCounts[54] and the resulting expression counts were used to compute differential expression statistics with edgeR[55; 56]. Normalized expression was computed as log2 CPM (counts per million), including a TMM normalization and batch effect correction. Comparisons were made between GROUPS . In all cases p-values were adjusted for multiple testing using the false discovery rate (FDR) correction of Benjamini and Hochberg[57]. Volcano plots (Fig. SX-XX) were generated within the R programming language. DEG (Differentially Expressed Genes) with an absolute Log_2FC (Log Fold Change) <+2 or <-2 and a q value of less than 0.05 were assigned to specific pathways using the KEGG and further grouped under seven functional categories: (1) Metabolism, (2) Cellular Processes, (3) Genetic Information Processing, (4) Environmental Processing, (5) Immune System and (6) Nervous System.

16S Microbiome Analyses. Details have been described by us previously[5]. Briefly, DNA was extracted from fecal samples using a Maxwell RSC48 device (Promega), with bead-beating implemented off-instrument. Microbial community structure was characterized by DNA extraction, PCR amplification and sequencing of 16S ribosomal RNA gene amplicons[58]. Raw sequence data was processed with *QIIME2*[59] and the *Vegan* bioinformatics package[60]. Inference of functional gene content was performed within the software package *PICRUSt2*[61]. Differential expression statistics was computed using edgeR[55; 56], on raw expression counts obtained from quantification. Normalized expression was computed as log2 CPM (counts per million), including a TMM normalization and batch effect correction. Comparisons were made between study groups. In all cases p-values were adjusted for multiple testing using the false discovery rate (FDR) correction of Benjamini and Hochberg[57].

RESULTS

Inflammation-Induced knee joint following IAI of CFA

To establish a time course of knee joint responses following CFA or PBS injections, CFA-IAI and Naïve rats were sacrificed at days 3, 7 and 14 post-IAI for analyses (**Fig. S1** and Methods). Knee joint swelling in the medial-lateral orientation had developed by 3d post-CFA-IAI and remained elevated through 14d ($p < 0.001$, 2-way ANOVA) compared to controls (**Fig. 1A**). There was a significant time effect with CFA-IAI ($p = 0.005$, 1 way ANOVA) as well as a time x study group interaction ($p = 0.008$, 2-way ANOVA).

The initial joint swelling response to CFA-IAI is likely the result of a transient increase in serum effusion into the joint space as indicated by accumulation of Bikunin in the synovial fluid was transiently elevated **(Fig. 1B)** with a concurrent decrease in circulating serum levels (**Fig. 1C,** $p = 0.002$, t-test). Electrophoretic analyses for serum proteins in the synovial fluid lavages showed an abundance of albumin and IgG at 3d post-CFA-IAI (**Fig. S2**). The increased serum components were no longer present at 14d post-CFA. The persistent increases in

CFA-induced knee diameters were likely due to joint tissue responses, such as hyperplasia and fibrotic remodeling of the synovium and patellar tendon swelling (**Figs. 1D-G**). By comparison, no alteration in joint fluid composition or tissue remodeling were noted after PBS-IAI.

Transient changes in metaphyseal bone following CFA-IAI

As reported by others[62-64], CFA-IAI resulted in robust periarticular bone loss in affected joints. Using micro-computed tomography, we detected distal femoral metaphyseal and epiphyseal bone changes in both the cortical and trabecular bone compartments. Cortical bone pitting was present at 3d post-CFA IAI in the proximal region of the patellar groove. By 7d the pitting was extended distally through the distal metaphysis to the epiphyses (**Fig. 2A**). Adjacent to the cortical pitting, periosteal reactions were present in n=7 7d and n=2 14d rats, primarily in the antero-mediolateral region of the distal femur (representative images in **Figs. 2B** & **S3**). These reactions occurred transiently coincident with the peak knee swelling, metaphyseal bone loss, and synovial fluid content of bikunin to CFA. By 14d with the cortex appeared smooth and the periosteal mineralization had infilled (**Fig. 2**). Interestingly, this phenotype did not show any significant treatment effects on cortical geometry measurements including cortical thickness ($p = 0.142$, 2-way ANOVA) or cortical area ($p = 0.271$, 2-way). Trabecular bone volume fraction was significantly decreased in the metaphysis with CFA-IAI (**Fig. 2C & D**). This decrease was due to significant decreases in both trabecular number and trabecular thickness with trabecular spacing significantly increasing (**Fig. 2D**). Trabecular changes persisted past the 7d peak of inflammation. The structural model index was significantly increased with CFA-IAI suggesting the shape of the trabeculae changed to be more cylindrical (SMI= 3) rather than planar (SMI= 1) with CFA-IAI. The connectivity density was significantly decreased with CFA-IAI suggesting that trabeculae were less connected with CFA treatment.

Bulk RNA Seq identifies transcriptomic responses of the knee joint synovium following IAI of CFA or PBS

Assessment of changes in tissue- or cell-specific transcriptomic landscapes has become an essential tool to identify and quantitate responses to disease-causing injurious toxic or infectious stimuli in a range of tissues, including intestine[65-68]. We have therefore applied bulk-RNASeq methodology and post-sequencing bioinformatics analyses to identify essential genes using the Database of Essential Genes (DEG) and associated pathway responses of synovial tissues to IAI of CFA or PBS (sham).

A global overview of gene expression profiles in synovium at 0d and post-CFA or PBS is shown in **Fig. 3A**. Whereas sham injections caused only minimal shifts (increased or decreased abundance) in gene expression profiles at 3d and 14d, CFA-IAI resulted in notably activated or depressed levels of expression at all timepoints up to 14d. DEGs at each post-IAI treatment timepoint, relative to 0d were calculated and significantly modified genes were outlined in the volcano plots (**Fig. 3B-F ;** red dots = activated >1.5 $\log_2$FC, p-value<0.05 or suppressed <-1.5 $\log_2$FC, $p<0.05$). Using 'significant fold change' selection parameters, CFA exposure upregulated transcript abundance for 592, 1037, and 998 genes at 3, 7 and 14d, respectively, but decreased transcripts for 167, 998 and 166 genes at the corresponding timepoints. By comparison, after sham-IAI-PBS,

increases relative to 0d occurred for 32 and 180 genes and suppression for 37 and 67 genes 3d and 14d, respectively.

The acute (3d) response to CFA-IAI resulted in limited but strong immune and inflammation responses, with >100 fold increases in transcripts of the neutrophil protein S1009[69], the macrophage receptor CLEC5A[70], and the pro-angiogenic protease MMP9[71] as well as the lymphocyte activating factor SLAMF6[72], and F2RL2 involved in T-cell-fibroblast crosstalk. Other acutely expressed DEG included *Il1b Il1rn Il1r2, Ccl3, Ccl9 and Cxcl1*. Multiple genes, including pro-inflammatory mediators (*Ccl3*[73], *Cxcl1*[74], *Ccl2*[75], *Ccl9*[76], *Nos2*[77], Il1rn[78], *Il1b*[79], *Gdf15*[80] and *Osm*[81]), their regulators (*S100a9*[82], *Slamf6*[83], *Il1r2*[84], *Clec5a*[84], *Clec4e*[85], *Lcn2*[86] and Otud7a[87]), proteases (*Adam8*[88]) and regulators of cell matrix interactions of synovial fibroblasts (*Itgb8*[89]) are associated with inflammatory arthritis and showed sustained modification up to 14d. However, transcripts for multiple genes with known functions in innervation and inflammatory pain (*Kcne5, Grin3a, Map2, Erc2, Serpini1, Gprin3, Trhde* and *Mdga2*) remained suppressed post-CFA.

Interestingly, the *Spp1* gene that encodes the bone protein OPN (osteopontin), binds tightly to hydroxyapatite to form an integral part of the mineralized matrix and acts as a cytokine in OA and RA-related synovial inflammation[90; 91]. In our dataset, it was the most highly activated gene at 3d post-PBS and -CFA with a sustained upregulation at 7d post-CFA.

Transcriptomic responses of the proximal and distal ileum and distal colon following IAI of CFA

Bulk RNASeq analyses was also performed for intestinal tissues collected at 3, 7 and 14d post-CFA IAI from the proximal and distal ileum and the distal colon. Bioinformatic analyses of sequencing data for DEGs, pathways, and biological process modifications were performed as described in the methods. It should be noted that since sham IAI-PBS did not yield significant modification of synovial gene transcriptions when compared to CFA exposure (**Fig. 3**), RNASeq analyses of gut tissues was only performed on Naïve and CFA-treated gut samples. Gene expression profiles and DEGs for all three intestinal regions (proximal and distal ileum and colon) are shown in **Figs. 4-6,** respectively. These show a wide range of transcriptional changes relative to d0, with statistically significant increases and decreases in DEGs ($<\log_2$-1.5 and $> \log_2$+1.5). To supplement the volcano plots in panels B-D, details of DEGs are also shown as heatmaps (**Figs. S3A-C & S4A-C)**. Together, these data show that changes in affected genes were region-specific and also varied with time post-CFA treatment. For example, maximum modifications of the proximal ileal transcriptome were seen at d7 post-CFA, compared to d3 for the colonic transcriptome, with the distal ileum showing a weaker and rather uniform response at all 3 post-CFA timepoints (**Fig. S3**).

Transcripts that were modified at more than one post-CFA time point in each of the three intestinal regions are summarized in **Fig. S4A-C**. In the proximal ileum, these included increases in *Mptx1*[92-97], a gut-specific member of the pentraxin family, which is expressed by Paneth cells and serves to bridge adaptive and innate immunities and associated inflammatory responses, *Adgrg2*[98], selectively expressed in immunoregulatory tuft cells and *Tmprss15*[99], which encodes enterokinase, a gastrointestinal enzyme responsible for regulation of

sodium and potassium absorption. In addition, several genes expressed by neutrophils (*Mpo*[100-102], *Mst1*[103; 104], *Plaat1)* have been shown to be involved in IBD pathologies also showed elevated expression at 7d and 14d. Decreased transcript abundance of genes encoding anti-microbial peptides, *Reg1a*[105], *Reg3b*[106] and *Reg3g*[107; 108] were present at both 3d and 7d. In the distal ileum, a strong and sustained response of epithelial cells was supported by increased transcripts for *Mptx1*[93], *Hoxa9*[109; 110], *Slc7a14*[111], *Cldn8*[112-114] as well as antimicrobial response by increased *Lyc2 (Lyzl-1)*[115] and *Rdh7*[116-118], which are involved in retinoic acid metabolism and downstream control of microbiome composition. Downregulated expression was seen for epithelial cell specific genes, involved in glucose transport and uptake, *Gpr17*[119], *Slc2a2*[120] and *Slc5a4* (*Sglt3*)[121].

The most profound transcriptional response to the CFA-induced joint inflammation were seen in the distal colon and resulted in decreased mRNA level for a wide range of genes (**Figs. S3C & S4C**). Downregulated transcripts were seen for genes involved in regulation of intestinal immune responses, including *Serpine1*[122], which modulates immune cell infiltration or *Cxcl11*[123; 124] and *Atf3*[125; 126], which play pivotal roles in activation of Th17 cells and controlling the production of Il-22 and Il-17A. Several of the identified transcripts also point to cell-specific modulations; the epithelial cell-associated genes include *Btnl8*[127; 128], *Fabp1*[129], *Prkg2*[130; 131], *Car1*[132] and *Dmbt1*[133; 134]; the myofibroblast associated genes include *Cxcl11*[123; 124] and *Nr4a1*[135; 136] the enteroendocrine cell specific gene *GcG*[137; 138] and *SlcC17a*[139], which encodes a glutamate transporter in enteric neurons. The small number of increased mRNAs were for transcription factors *EyA1*[140] and *Tbx5*[141] both of which have been implicated in cell proliferation and EMT in colon cancers. It should also be noted that only few DEGs in intestinal responses overlapped with those seen in the synovium. *Nos2, S100a9, Cxcl1, Ccl2, and Lcn2* were increased in the synovium and decreased in the intestine, whereas *C1ql3* and *Serpine1a* were decreased in the synovium and increased in the intestine.

Pathway and biological process allocation of DEGs using GO enrichment

To assign a functional significance of modified gene transcripts within the context of cellular pathways in synovium and intestinal tissues, GO enrichment analyses was performed using the KEGG pathway database. Individual pathways were further assigned to the following six biological processes listed in that database: Metabolism, Cellular Processes, Genetic Information Processing, Environmental Processing, Immune System and Nervous System. Note that all gene sets with a log FC value of <-0.3 and >+0.3, and an adjusted p-value <0.05, were included. The data are displayed in dot plots for synovium (**Figs. S5 & S6**), proximal ileum (**Fig. S7**), distal ileum (**Fig. S8**) and distal colon (**Fig. S9**) and are also summarized in Venn diagrams (**Figs. 7&8**) Following CFA-IAI, a large number of pathways were activated in synovial tissue (**Figs. 7A and S5A**) (i.e., 45, 40 and 37 at 3d, 7d and 14d, respectively) or suppressed (i.e. 22, 32 and 6 at 3d, 7d and 14d, respectively). As expected from previous reports of the CFA model[38; 39], the adjuvant produced robust and persistent immune and inflammatory reactions in the synovium. Activated pathways included “NK cell mediated cytotoxicity”, “Neutrophil extracellular trap formation” “Th1 and Th2 cell differentiation”, “Th17 cell differentiation” and “B cell receptor signaling” pathways at 3d, 7d and 14d post-CFA exposure. This was accompanied by a stimulation of “Toll-like-

receptor”-, “C-type lectin-” “IL17-” and “NOD-like”-immune cell signaling characteristic of immune cells. Other inflammation-related pathways such as of “cytokine–cytokine receptor interactions”, “chemokine signaling” and “Nf-kappaB signal transduction” were also stimulated. Throughout the post-CFA period examined, a range of other pathways was suppressed, such as the Hippo pathway[142; 143], which can lead to induction of cell division and the suppression apoptosis by PPAR signaling[144], and this is expected to interfere with control of the inflammatory response to TNF-α in synovial cells[144]. Other notable adjuvant activated responses were seen in lysosomal, phagosomal, apoptotic, and necroptotic pathways, while neuronal system pathways such as “axon guidance” and “glutamatergic synapse function” were suppressed. By comparison, PBS-IAI resulted in a very minimal response of the synovium. The only modified pathways that showed overlap with those modified by CFA were “heparan sulfate biosynthesis”, “RNA polymerase” and “tryptophan metabolism” at 3d and “neuroactive ligand-receptor interaction”, “HIF-1 and calcium signaling” pathways at 14d, but no immune or inflammation related pathways were changed. A mild sham-IAI response was expected and has been reported in the clinical setting for sham injection[145] or joint space lavage[146].

The corresponding GO analyses of intestinal tissues **(Figs. 8 & S6, S7, S8)** showed fewer affected pathways than those identified in the synovium. As expected from the extensively downregulated transcriptome (**Figs. 4-6**) after CFA-IAI, many of the identified pathways were suppressed, most notably those associated with the immune system. In the proximal ileum, “Th1 and Th2 cell differentiation”, “Natural killer cell mediated cytotoxicity”, “Th17 cell differentiation”, and “Antigen processing and presentation” were suppressed over the entire experimental timeline. In the distal ileum, the “Intestinal immune network for IgA production” and the “Antigen processing and presentation” pathways were suppressed at 7d and 14d. These immune pathways were also suppressed in the distal colon, together with “B cell receptor” and “T cell receptor- signaling, and “Leukocyte trans endothelial migration”. Transcripts for a range of metabolic pathways and signaling pathways were also decreased in both the ileum and colon.

A comparison of pathway-specific responses between synovial and intestinal tissues, is shown in **Fig. 9.** Although many of the same pathways were affected, activation responses in the synovium gave corresponding suppression responses in the intestinal tissues, and this was particularly evident during the peak joint inflammation responses at 3d and 7d. This, together with the DEG data, confirms a generalized ‘silencing’ of inflammatory and immune reactions in the intestine. This likely constitutes a shielding response to maintain intestinal barrier function in the presence of an acute innate immune and inflammatory insult at a remote tissue site.

Effect of IAI of CFA on intestinal mucins, immune cells and Digestive Functions and Microbiome Composition

In keeping with the gut protective response including microbial immune activation we observed increased secretion of mucins with altered oligosaccharide structures by alcian blue histology and lectin immunochemistry. (**Fig. 10A**). It was accompanied by increased transcript abundance for core proteins of MUC1, 2, 4 and 5b as well as the goblet cell specific sialyl transferase ST6GALNAC1[31] (**Fig. 10B**).

Based on our RNASeq data, several digestive system pathways throughout the different regions of the intestine were affected by the inflammatory response of the knee joint. For example, transcripts encoded by genes associated with 'mineral absorption" were modulated in all 3 regions of intestine and were largely decreased compared to Naive. The distal colon showed suppression of the fat digestion pathways, with decreases in expression of 4 associated genes **(Fig. 12A).**

Interestingly, there was no evidence for development of dysbiosis in the model. The fecal microbiota from the distal ileum and colon were minimally altered in response to the knee joint inflammation and respective intestinal cell responses. Alpha diversity for within-group comparison was unaltered, as shown by evenness ($p = 0.697$), Shannon index ($p = 0.997$), and Simpson index ($p = 0.998$). Relative bacterial abundance (>1%) for the distal ileum and the colon (**Fig. 12B**) at the phylum level showed a slight shift from Naïve to 3d, 7d and 14d post-CFA IAI. Amongst this shift, there was a decrease in *Romboustia* in the ileum at 3d post-CFA, followed by an increase at 7d and a return to naïve levels by 14d. *Lactobacilus* showed the opposite shift with an increase by 3d, decrease by 7d and a return to naïve levels by 14d. This change in abundance supports a mild and importantly, a limited transient response of the microbiome when acute inflammation in the joint peaks at 7d post-CFA-IAI. Due to the observation of a transient change in mucus layer 16S data were mined for the abundance of mucin-degrading bacteria (*Akkermansia, Alistipes*) and sialic acid cleaving bacteria (*Bifidobacterium*) (**Fig. S10**). Apart from the appearance of a low levels of *Akkermansia* in the feces from distal ileum and distal colon post IAI of CFA, the joint inflammation had not detectable effect on the other two species.

DISCUSSION

The CFA mono-joint RA model results in an acute joint inflammation that is induced after injection of inactive mycobacterium suspended in adjuvant, into ankle, knee or TMJ joints of skeletally mature mice or rats[39; 147] has been used widely to examine pain[148; 149], and joint-tissue inflammatory responses. Due to its reproducibility and rapid response, it has also been applied in preclinical testing of a wide range of disease modifying RA drugs[150; 151]. Most recently it was shown to be a suitable model to study cross-talk between joint and the myocardial system seen in RA[152]. Together, these studies support the suitability of this model for our novel studies to examine the molecular and cell biological responses of the gut to joint inflammation.

Arthritis symptoms are typically assessed by joint swelling measurements, histology of joint tissues and µCT for bone structural changes[153; 154]. Intestinal response measurements include 16S RNA assessment of the fecal microbiome and intestinal barrier functions determined by tight junction protein IHC and gut permeability to different molecular weight dextran polymers. However, a comprehensive assessment of time-dependent cellular and molecular biological changes during development of the inflammatory response and formation of a synovial pannus have been limited. Likewise no information is available about the timing of intestinal responses to those occurring in the joint, and whether there is coordinated modulation of intestinal homeostasis by common pathway changes in inflammatory, immune and neuronal pathways in the synovium.

To gain novel information on such a possible joint-gut communication in the CFA model, we first established a timeframe for post-CFA inflammatory responses of the joint. An early and robust response to the adjuvant occurred at 3d and 7d, indicated by joint space effusion and bone damage which was followed by the formation of a fibrotic myeloid infiltrated synovial pannus and a persistent change in metaphyseal trabecular architecture in the presence of a transient periosteal response at 14d. The gross evaluation of the time-sensitive joint inflammation responses were supported by bulk RNASeq analyses of the synovial tissue. To minimize difficulties in result interpretation due to potential sampling errors of synovium from the rat knee joint, tissues were collected from the readily identifiable peri-meniscal sites and included the patellar fat pad. Thus transcriptional regulation of pro-inflammatory and immune pathways were seen throughout the 14d post-CFA period for all genes that had increases or decreases in in transcript abundance.

RNASeq analyses of proximal and distal regions of the Ileum suggest that a range of cell types in the intestinal barrier were affected, including epithelial, Paneth, goblet and Tuft cells, with minimal response from T cells or macrophages (**Fig. 11**). Epithelial and goblet cell associated transient changes in mucin metabolism, post-CFA were further supported by lectin histochemistry and modulated mRNA abundance of mucin core protein and glycosylation enzymes (**Fig. 10**).

Most remarkable however was the finding that based on both DEG and GO analyses a wide range of immune and inflammatory genes and pathways, which were strongly and persistently activated in the synovium were suppressed in the ileum as well as the colon. However, it should be noted that the transcriptomic assay at each timepoint only provides data for a narrow window during a continued progressive process of post-CFA responses. Thus, increased transcript levels could also arise from slower translation or decreased degradation of a given mRNA, and conversely from high levels of translation or increased mRNA turnover. Therefore interpretation of transcript levels in terms of activated or suppressed translation of genes would require application of methods such as ATACSeq[155] to identify regions of the genome that are accessible or blocked and to what extend epigenetic modulation of gene expression plays a role in inter-organ communication in chronic inflammation.

Transmission of signals between diseased tissues and the gut has been postulated for a wide range of disease conditions, but the molecular and cell biological mechanisms remain largely undefined, except for the much-studied interactions between the brain, intestine, and microbiome[156]. The communication channels include inflammatory cell products (cytokine/chemokines), migrating or circulating immune cells (T-cells, macrophages) as well as microbiota- derived metabolites. Our data do not support a prominent role of cross activation of, or infiltration of, immune cells into the intestinal tissues (**Fig. 10**) nor does the microbiome show much significant alterations post-CFA that would indicate dysbiosis or breakdown of the intestinal barrier function following the induction of a strong inflammatory response in the knee joint.

One possible route of inter-organ signal transmission involves the enteric nervous system (ENS), a highly conserved network of neuron and glial cells located within the walls of the intestinal tract that coordinate digestive processes and importantly control gastrointestinal homeostasis[157]. It has been shown to play a role in the gut-

brain axis in neurodegenerative disorders[158]. In the context of this study, it has been indicated in the development of gut inflammation and dysbiosis in response to psychological stress such as pain-induced anxiety[159; 160] that are likely present in the CFA joint inflammation model. Indeed, our data suggest a likely neurobiological involvement in the intestinal response to joint inflammation induced by CFA-IAI. Thus, neuronal pathways are amongst the activated pathways throughout the post-CFA induced responses. Such a response was seen in all three regions of the intestine (**Fig. S7-9**), but predominant in the ileum. Such pathways include serotonergic[161] and glutamatergic synapses[162], and synaptic vesicle recycling and retrograde endocannabinoid signaling[163]. In addition, transcripts of genes with known neurobiological effects, such *Gdf15*[164], *Atp1a3*[165], and *Mdga2*[166] were modulated.

In summary, we provide for the first time a comprehensive analysis of a potential temporally coordinated response between the synovium and the intestine to CFA-IAI into healthy knee joints of skeletally mature rats. The data show a suppression of immune and inflammatory pathways in the ileum and colon, when such pathways are highly activated in the synovium. This suggests that the intestine mounts a protective response to offset any damage to the intestinal barrier, primarily within the immune cell population and the homeostatic composition of the microbiome. However, the indication of cell-specific responses in both the small intestine and colon necessitate further studies to identify the cell-specific and spatial distribution of the transcriptomic responses in the intestinal tissues[167]. In addition, further evidence for a modulation of ENS function by pain responses in models of inflammatory and degenerative joint diseases should be examined in other *in vivo* models. This would allow for deep understanding of chronic disease and used in combination with administration of therapeutics that target inflammatory pain in these models.

Acknowledgements

We would like to thank Dr. Georgia Papavasiliou (Illinois Institute of Technology) and Dr. Joseph Reynold (Rosalind Franklin University) for their insightful discussions during the progression of this project, Phillip Engen (Rush) for support with microbiome data analysis and Rylan Martin for technical support. Funding for this project is from the Department of Orthopedic Surgery, RUMC (MMM) and the Katz/Rubschlager Endowed Chair at RUMC (AP).

References

1. Hernandez CJ, Guss JD, Luna M, et al. 2016. Links Between the Microbiome and Bone. J Bone Miner Res 31:1638-1646.
2. Scher JU, Littman DR, Abramson SB. 2016. Microbiome in Inflammatory Arthritis and Human Rheumatic Diseases. Arthritis Rheumatol 68:35-45.
3. Holloway L, Moynihan S, Abrams SA, et al. 2007. Effects of oligofructose-enriched inulin on intestinal absorption of calcium and magnesium and bone turnover markers in postmenopausal women. The British journal of nutrition 97:365-372.
4. Seely KD, Kotelko CA, Douglas H, et al. 2021. The Human Gut Microbiota: A Key Mediator of Osteoporosis and Osteogenesis. Int J Mol Sci 22.
5. Moran MM, Wilson BM, Li J, et al. 2020. The gut microbiota may be a novel pathogenic mechanism in loosening of orthopedic implants in rats. FASEB J 34:14302-14317.

6. Kalinkovich A, Livshits G. 2019. A cross talk between dysbiosis and gut-associated immune system governs the development of inflammatory arthropathies. Semin Arthritis Rheum 49:474-484.
7. Zhang L, Hu Y, Xu Y, et al. 2019. The correlation between intestinal dysbiosis and the development of ankylosing spondylitis. Microb Pathog 132:188-192.
8. Favazzo LJ, Hendesi H, Villani DA, et al. 2020. The gut microbiome-joint connection: implications in osteoarthritis. Curr Opin Rheumatol 32:92-101.
9. Scheithauer TPM, Rampanelli E, Nieuwdorp M, et al. 2020. Gut Microbiota as a Trigger for Metabolic Inflammation in Obesity and Type 2 Diabetes. Front Immunol 11:571731.
10. Rosendo-Silva D, Viana S, Carvalho E, et al. 2023. Are gut dysbiosis, barrier disruption, and endotoxemia related to adipose tissue dysfunction in metabolic disorders? Overview of the mechanisms involved. Intern Emerg Med 18:1287-1302.
11. Nesci A, Carnuccio C, Ruggieri V, et al. 2023. Gut Microbiota and Cardiovascular Disease: Evidence on the Metabolic and Inflammatory Background of a Complex Relationship. Int J Mol Sci 24.
12. Li S, Zhao L, Xiao J, et al. 2024. The gut microbiome: an important role in neurodegenerative diseases and their therapeutic advances. Mol Cell Biochem 479:2217-2243.
13. Saxami G, Kerezoudi EN, Eliopoulos C, et al. 2023. The Gut-Organ Axis within the Human Body: Gut Dysbiosis and the Role of Prebiotics. Life (Basel) 13.
14. Hou K, Wu ZX, Chen XY, et al. 2022. Microbiota in health and diseases. Signal Transduct Target Ther 7:135.
15. Malesza IJ, Malesza M, Walkowiak J, et al. 2021. High-Fat, Western-Style Diet, Systemic Inflammation, and Gut Microbiota: A Narrative Review. Cells 10.
16. Vich Vila A, Collij V, Sanna S, et al. 2020. Impact of commonly used drugs on the composition and metabolic function of the gut microbiota. Nat Commun 11:362.
17. He J, Guo H, Zheng W, et al. 2019. Effects of Stress on the Mucus-microbial Interactions in the Gut. Curr Protein Pept Sci 20:155-163.
18. Proffitt C, Bidkhori G, Moyes D, et al. 2020. Disease, Drugs and Dysbiosis: Understanding Microbial Signatures in Metabolic Disease and Medical Interventions. Microorganisms 8.
19. Vancamelbeke M, Vermeire S. 2017. The intestinal barrier: a fundamental role in health and disease. Expert Rev Gastroenterol Hepatol 11:821-834.
20. Inaba R, Vujakovic S, Bergstrom K. 2023. The gut mucus network: A dynamic liaison between microbes and the immune system. Semin Immunol 69:101807.
21. Salvo Romero E, Alonso Cotoner C, Pardo Camacho C, et al. 2015. The intestinal barrier function and its involvement in digestive disease. Rev Esp Enferm Dig 107:686-696.
22. Li J, Jia N, Cui M, et al. 2023. The intestinal mucosal barrier - A key player in rheumatoid arthritis? Clin Anat.
23. Matei DE, Menon M, Alber DG, et al. 2021. Intestinal barrier dysfunction plays an integral role in arthritis pathology and can be targeted to ameliorate disease. Med 2:864-883.e869.
24. Tajik N, Frech M, Schulz O, et al. 2020. Targeting zonulin and intestinal epithelial barrier function to prevent onset of arthritis. Nat Commun 11:1995.
25. Wen J, Lyu P, Stolzer I, et al. 2022. Epithelial HIF2α expression induces intestinal barrier dysfunction and exacerbation of arthritis. Ann Rheum Dis.
26. Lyu P, Wen J, Zhang W, et al. 2024. Expression of HIF1α in intestinal epithelium restricts arthritis inflammation by inhibiting RIPK3-induced cell death machinery. Ann Rheum Dis 83:984-997.
27. Kalliolias GD, Papavassiliou AG. 2024. Stabilizing the integrity of intestinal barrier to control arthritis. Arthritis Res Ther 26:135.
28. Bevins CL, Salzman NH. 2011. Paneth cells, antimicrobial peptides and maintenance of intestinal homeostasis. Nat Rev Microbiol 9:356-368.
29. Pelaseyed T, Bergström JH, Gustafsson JK, et al. 2014. The mucus and mucins of the goblet cells and enterocytes provide the first defense line of the gastrointestinal tract and interact with the immune system. Immunol Rev 260:8-20.
30. Fekete E, Buret AG. 2023. The role of mucin O-glycans in microbiota dysbiosis, intestinal homeostasis, and host-pathogen interactions. Am J Physiol Gastrointest Liver Physiol 324:G452-g465.
31. Yao Y, Kim G, Shafer S, et al. 2022. Mucus sialylation determines intestinal host-commensal homeostasis. Cell 185:1172-1188.e1128.

32. Lo Conte M, Cosorich I, Ferrarese R, et al. 2023. Alterations of the intestinal mucus layer correlate with dysbiosis and immune dysregulation in human Type 1 Diabetes. EBioMedicine 91:104567.
33. Xu L, Chang C, Jiang P, et al. 2022. Metabolomics in rheumatoid arthritis: Advances and review. Front Immunol 13:961708.
34. Hirata I, Berrebi G, Austin LL, et al. 1986. Immunohistological characterization of intraepithelial and lamina propria lymphocytes in control ileum and colon and in inflammatory bowel disease. Dig Dis Sci 31:593-603.
35. Yan JB, Luo MM, Chen ZY, et al. 2020. The Function and Role of the Th17/Treg Cell Balance in Inflammatory Bowel Disease. J Immunol Res 2020:8813558.
36. Saez A, Gomez-Bris R, Herrero-Fernandez B, et al. 2021. Innate Lymphoid Cells in Intestinal Homeostasis and Inflammatory Bowel Disease. Int J Mol Sci 22.
37. Diefenbach A, Gnafakis S, Shomrat O. 2020. Innate Lymphoid Cell-Epithelial Cell Modules Sustain Intestinal Homeostasis. Immunity 52:452-463.
38. Freund J. 1947. SOME ASPECTS OF ACTIVE IMMUNIZATION. Annual Review of Microbiology 1:291-308.
39. Uematsu T, Sakai A, Ito H, et al. 2011. Intra-articular administration of tachykinin NK1 receptor antagonists reduces hyperalgesia and cartilage destruction in the inflammatory joint in rats with adjuvant-induced arthritis. European Journal of Pharmacology 668:163-168.
40. Siddique R, Muhammad F, Faisal MN, et al. 2024. Gingerol nanoparticles attenuate complete Freund adjuvant-induced arthritis in rats via targeting the RANKL/OPG signaling pathway. Inflammopharmacology 32:3311-3326.
41. Bhattaram P, Chandrasekharan U. 2017. The joint synovium: A critical determinant of articular cartilage fate in inflammatory joint diseases. Semin Cell Dev Biol 62:86-93.
42. Gardner DL. 1994. Problems and paradigms in joint pathology. J Anat 184 (Pt 3):465-476.
43. Furuzawa-Carballeda J, Macip-Rodríguez PM, Cabral AR. 2008. Osteoarthritis and rheumatoid arthritis pannus have similar qualitative metabolic characteristics and pro-inflammatory cytokine response. Clin Exp Rheumatol 26:554-560.
44. Wang X, Liu D, Li D, et al. 2023. Combined treatment with glucosamine and chondroitin sulfate improves rheumatoid arthritis in rats by regulating the gut microbiota. Nutr Metab (Lond) 20:22.
45. Chen X, Wang J, He Z, et al. 2022. Analgesic and Anxiolytic Effects of Gastrodin and Its Influences on Ferroptosis and Jejunal Microbiota in Complete Freund's Adjuvant-Injected Mice. Front Microbiol 13:841662.
46. Liu M, Li S, Cao N, et al. 2023. Intestinal flora, intestinal metabolism, and intestinal immunity changes in complete Freud's adjuvant-rheumatoid arthritis C57BL/6 mice. Int Immunopharmacol 125:111090.
47. Bialkowska AB, Ghaleb AM, Nandan MO, et al. 2016. Improved Swiss-rolling Technique for Intestinal Tissue Preparation for Immunohistochemical and Immunofluorescent Analyses. Journal of visualized experiments : JoVE.
48. Julie Le Naour; Léa Montégut; Adrien Joseph; Kévin Garbind EVGKJGPMCM. 2022. Improved Swiss-rolling method for histological analyses of colon tissue. MethodsX 9.
49. Xue J, Chen J, Shen Q, et al. 2020. Addition of High Molecular Weight Hyaluronic Acid to Fibroblast-Like Stromal Cells Modulates Endogenous Hyaluronic Acid Metabolism and Enhances Proteolytic Processing and Secretion of Versican. Cells 9.
50. Schneider CA, Rasband WS, Eliceiri KW. 2012. NIH Image to ImageJ: 25 years of image analysis. Nat Methods 9:671-675.
51. Chan DD, Li J, Luo W, et al. 2018. Pirfenidone reduces subchondral bone loss and fibrosis after murine knee cartilage injury. J Orthop Res 36:365-376.
52. Martin M. 2011. Cutadapt removes adapter sequences from high-throughput sequencing reads. EMBnetjournal 17:10-12.
53. Dobin A, Davis CA, Schlesinger F, et al. 2013. STAR: ultrafast universal RNA-seq aligner. Bioinformatics 29:15-21.
54. Liao Y, Smyth GK, Shi W. 2014. featureCounts: an efficient general purpose program for assigning sequence reads to genomic features. Bioinformatics 30:923-930.
55. McCarthy DJ, Chen Y, Smyth GK. 2012. Differential expression analysis of multifactor RNA-Seq experiments with respect to biological variation. Nucleic Acids Res 40:4288-4297.

56. Robinson MD, McCarthy DJ, Smyth GK. 2010. edgeR: a Bioconductor package for differential expression analysis of digital gene expression data. Bioinformatics 26:139-140.
57. Benjamini Y, Hochberg Y. 1995. Controlling the False Discovery Rate: A Practical and Powerful Approach to Multiple Testing. Journal of the Royal Statistical Society: Series B (Methodological) 57:289-300.
58. Naqib A, Poggi S, Wang W, et al. 2018. Making and Sequencing Heavily Multiplexed, High-Throughput 16S Ribosomal RNA Gene Amplicon Libraries Using a Flexible, Two-Stage PCR Protocol. Methods Mol Biol 1783:149-169.
59. Bolyen E, Rideout JR, Dillon MR, et al. 2019. Reproducible, interactive, scalable and extensible microbiome data science using QIIME 2. Nat Biotechnol 37:852-857.
60. Okasanen J, Kindt R, Legendre P, et al. 2007. The vegan package. Community ecology package 10.
61. Douglas GM, Maffei VJ, Zaneveld JR, et al. 2020. PICRUSt2 for prediction of metagenome functions. Nat Biotechnol 38:685-688.
62. Vermeirsch H, Biermans R, Salmon PL, et al. 2007. Evaluation of pain behavior and bone destruction in two arthritic models in guinea pig and rat. Pharmacol Biochem Behav 87:349-359.
63. Wu G, Nie W, Wang Q, et al. 2021. Umbelliferone Ameliorates Complete Freund Adjuvant-Induced Arthritis via Reduction of NF-κB Signaling Pathway in Osteoclast Differentiation. Inflammation 44:1315-1329.
64. Nagae M, Hiraga T, Wakabayashi H, et al. 2006. Osteoclasts play a part in pain due to the inflammation adjacent to bone. Bone 39:1107-1115.
65. Chen Y, Agellon LB. 2020. Distinct Alteration of Gene Expression Programs in the Small Intestine of Male and Female Mice in Response to Ablation of Intestinal Fabp Genes. Genes (Basel) 11.
66. Su Y, Zhang X, Liang Y, et al. 2024. Integrated analysis of single-cell RNA-seq and bulk RNA-seq to unravel the molecular mechanisms underlying the immune microenvironment in the development of intestinal-type gastric cancer. Biochim Biophys Acta Mol Basis Dis 1870:166849.
67. Zhang T, Yan M, Chang M, et al. 2024. Integrated transcriptomics and metabolomics reveal the mechanism of intestinal damage upon acute patulin exposure in mice. Ecotoxicol Environ Saf 276:116270.
68. Burge K, Eckert J, Wilson A, et al. 2022. Hyaluronic Acid 35 kDa Protects against a Hyperosmotic, Formula Feeding Model of Necrotizing Enterocolitis. Nutrients 14.
69. Parisien M, Lima LV, Dagostino C, et al. 2022. Acute inflammatory response via neutrophil activation protects against the development of chronic pain. Sci Transl Med 14:eabj9954.
70. Sung PS, Chang WC, Hsieh SL. 2020. CLEC5A: A Promiscuous Pattern Recognition Receptor to Microbes and Beyond. Adv Exp Med Biol 1204:57-73.
71. Zhou M, Qin S, Chu Y, et al. 2014. Immunolocalization of MMP-2 and MMP-9 in human rheumatoid synovium. Int J Clin Exp Pathol 7:3048-3056.
72. Gartshteyn Y, Askanase AD, Mor A. 2021. SLAM Associated Protein Signaling in T Cells: Tilting the Balance Toward Autoimmunity. Front Immunol 12:654839.
73. Yang YL, Li XF, Song B, et al. 2023. The Role of CCL3 in the Pathogenesis of Rheumatoid Arthritis. Rheumatol Ther 10:793-808.
74. Hou SM, Chen PC, Lin CM, et al. 2020. CXCL1 contributes to IL-6 expression in osteoarthritis and rheumatoid arthritis synovial fibroblasts by CXCR2, c-Raf, MAPK, and AP-1 pathway. Arthritis Res Ther 22:251.
75. Moadab F, Khorramdelazad H, Abbasifard M. 2021. Role of CCL2/CCR2 axis in the immunopathogenesis of rheumatoid arthritis: Latest evidence and therapeutic approaches. Life Sci 269:119034.
76. Dawes JM, Kiesewetter H, Perkins JR, et al. 2013. Chemokine expression in peripheral tissues from the monosodium iodoacetate model of chronic joint pain. Mol Pain 9:57.
77. Maurer M, von Stebut E. 2004. Macrophage inflammatory protein-1. Int J Biochem Cell Biol 36:1882-1886.
78. Levescot A, Chang MH, Schnell J, et al. 2021. IL-1β-driven osteoclastogenic Tregs accelerate bone erosion in arthritis. J Clin Invest 131.
79. Rong H, He X, Wang L, et al. 2020. Association between IL1B polymorphisms and the risk of rheumatoid arthritis. Int Immunopharmacol 83:106401.

80. Esalatmanesh K, Fayyazi H, Esalatmanesh R, et al. 2020. The association between serum levels of growth differentiation factor-15 and rheumatoid arthritis activity. Int J Clin Pract 74:e13564.
81. Han L, Yan J, Li T, et al. 2023. Multifaceted oncostatin M: novel roles and therapeutic potential of the oncostatin M signaling in rheumatoid arthritis. Front Immunol 14:1258765.
82. Cesaro A, Anceriz N, Plante A, et al. 2012. An inflammation loop orchestrated by S100A9 and calprotectin is critical for development of arthritis. PLoS One 7:e45478.
83. Kwon YC, Lim J, Bang SY, et al. 2020. Genome-wide association study in a Korean population identifies six novel susceptibility loci for rheumatoid arthritis. Ann Rheum Dis 79:1438-1445.
84. Ocskó T, Tóth DM, Hoffmann G, et al. 2018. Transcription factor Zbtb38 downregulates the expression of anti-inflammatory IL1r2 in mouse model of rheumatoid arthritis. Biochim Biophys Acta Gene Regul Mech 1861:1040-1047.
85. Takata K, Takano S, Miyagi M, et al. 2021. Elevated macrophage-inducible C-type lectin expression in the synovial tissue of patients with rheumatoid arthritis. Cent Eur J Immunol 46:470-473.
86. Gulkesen A, Akgol G, Poyraz AK, et al. 2017. Lipocalin 2 as a clinical significance in rheumatoid arthritis. Cent Eur J Immunol 42:269-273.
87. Kasher M, Williams FMK, Freidin MB, et al. 2022. Understanding the complex genetic architecture connecting rheumatoid arthritis, osteoporosis and inflammation: discovering causal pathways. Hum Mol Genet 31:2810-2819.
88. Wang Z, Li W, Chen S, et al. 2023. Role of ADAM and ADAMTS proteases in pathological tissue remodeling. Cell Death Discov 9:447.
89. van Caam A, Aarts J, van Ee T, et al. 2020. TGFβ-mediated expression of TGFβ-activating integrins in SSc monocytes: disturbed activation of latent TGFβ? Arthritis Res Ther 22:42.
90. Martín-Márquez BT, Sandoval-García F, Corona-Meraz FI, et al. 2023. Osteopontin: A Bone-Derived Protein Involved in Rheumatoid Arthritis and Osteoarthritis Immunopathology. Biomolecules 13.
91. Wang Q, Wang W, Zhang F, et al. 2017. NEAT1/miR-181c Regulates Osteopontin (OPN)-Mediated Synoviocyte Proliferation in Osteoarthritis. J Cell Biochem 118:3775-3784.
92. van der Meer-van Kraaij C, Siezen R, Kramer E, et al. 2007. Dietary modulation and structure prediction of rat mucosal pentraxin (Mptx) protein and loss of function in humans. Genes Nutr 2:275-285.
93. Drew JE, Farquharson AJ, Keijer J, et al. 2006. Complex regulation of mucosal pentraxin (Mptx) revealed by discrete micro-anatomical locations in colon. Biochim Biophys Acta 1762:844-848.
94. Van Der Meer-Van Kraaij C, Van Lieshout EM, Kramer E, et al. 2003. Mucosal pentraxin (Mptx), a novel rat gene 10-fold down-regulated in colon by dietary heme. Faseb j 17:1277-1285.
95. Balasubramanian I, Bandyopadhyay S, Flores J, et al. 2023. Infection and inflammation stimulate expansion of a CD74(+) Paneth cell subset to regulate disease progression. Embo j 42:e113975.
96. Yan W, Chen S, Wang Y, et al. 2024. Loss of Mptx2 alters bacteria composition and intestinal homeostasis potentially by impairing autophagy. Commun Biol 7:94.
97. Li Y, Zhang S, Liu J, et al. 2023. The pentraxin family in autoimmune disease. Clin Chim Acta 551:117592.
98. Grunddal KV, Tonack S, Egerod KL, et al. 2021. Adhesion receptor ADGRG2/GPR64 is in the GI-tract selectively expressed in mature intestinal tuft cells. Mol Metab 51:101231.
99. Stacey D, Suppiah V, Benyamin B, et al. 2024. In-silico functional analyses identify TMPRSS15-mediated intestinal absorption of lithium as a modulator of lithium response in bipolar disorder. J Affect Disord 358:416-421.
100. Dos Santos Ramos A, Viana GCS, de Macedo Brigido M, et al. 2021. Neutrophil extracellular traps in inflammatory bowel diseases: Implications in pathogenesis and therapeutic targets. Pharmacol Res 171:105779.
101. Chami B, Martin NJJ, Dennis JM, et al. 2018. Myeloperoxidase in the inflamed colon: A novel target for treating inflammatory bowel disease. Archives of biochemistry and biophysics 645:61-71.
102. Schroder AL, Chami B, Liu Y, et al. 2022. Neutrophil Extracellular Trap Density Increases With Increasing Histopathological Severity of Crohn's Disease. Inflammatory bowel diseases 28:586-598.
103. Li T, Wen Y, Lu Q, et al. 2023. MST1/2 in inflammation and immunity. Cell Adh Migr 17:1-15.
104. Hong AW, Meng Z, Guan KL. 2016. The Hippo pathway in intestinal regeneration and disease. Nat Rev Gastroenterol Hepatol 13:324-337.

105. Sun C, Wang X, Hui Y, et al. 2021. The Potential Role of REG Family Proteins in Inflammatory and Inflammation-Associated Diseases of the Gastrointestinal Tract. Int J Mol Sci 22.
106. van Ampting MT, Loonen LM, Schonewille AJ, et al. 2012. Intestinally secreted C-type lectin Reg3b attenuates salmonellosis but not listeriosis in mice. Infection and immunity 80:1115-1120.
107. Shin JH, Bozadjieva-Kramer N, Shao Y, et al. 2022. The gut peptide Reg3g links the small intestine microbiome to the regulation of energy balance, glucose levels, and gut function. Cell Metab 34:1765-1778.e1766.
108. Greenhill C. 2023. REG3G - a potential link between the intestinal microbiome and host physiology. Nat Rev Endocrinol 19:5.
109. Duluc I, Lorentz O, Fritsch C, et al. 1997. Changing intestinal connective tissue interactions alters homeobox gene expression in epithelial cells. J Cell Sci 110 (Pt 11):1317-1324.
110. Doodnath R, Wride M, Puri P. 2012. The spatio-temporal patterning of Hoxa9 and Hoxa13 in the developing zebrafish enteric nervous system. Pediatr Surg Int 28:115-121.
111. Jiang X, Liu K, Jiang H, et al. 2023. SLC7A14 imports GABA to lysosomes and impairs hepatic insulin sensitivity via inhibiting mTORC2. Cell Rep 42:111984.
112. Li M, Zhao J, Cao M, et al. 2020. Mast cells-derived MiR-223 destroys intestinal barrier function by inhibition of CLDN8 expression in intestinal epithelial cells. Biol Res 53:12.
113. De Lisle RC. 2014. Disrupted tight junctions in the small intestine of cystic fibrosis mice. Cell and tissue research 355:131-142.
114. Wang H, Chao K, Ng SC, et al. 2016. Pro-inflammatory miR-223 mediates the cross-talk between the IL23 pathway and the intestinal barrier in inflammatory bowel disease. Genome Biol 17:58.
115. He JW, Zhou XJ, Li YF, et al. 2021. Associations of Genetic Variants Contributing to Gut Microbiota Composition in Immunoglobin A Nephropathy. mSystems 6.
116. Grizotte-Lake M, Zhong G, Duncan K, et al. 2018. Commensals Suppress Intestinal Epithelial Cell Retinoic Acid Synthesis to Regulate Interleukin-22 Activity and Prevent Microbial Dysbiosis. Immunity 49:1103-1115.e1106.
117. Xu TC, Lv Y, Liu QY, et al. 2022. Long-term atorvastatin improves cognitive decline by regulating gut function in naturally ageing rats. Immun Ageing 19:52.
118. Cao YG, Bae S, Villarreal J, et al. 2022. Faecalibaculum rodentium remodels retinoic acid signaling to govern eosinophil-dependent intestinal epithelial homeostasis. Cell host & microbe 30:1295-1310.e1298.
119. Yan S, Conley JM, Reilly AM, et al. 2022. Intestinal Gpr17 deficiency improves glucose metabolism by promoting GLP-1 secretion. Cell Rep 38:110179.
120. Morrice N, Vainio S, Mikkola K, et al. 2023. Metformin increases the uptake of glucose into the gut from the circulation in high-fat diet-fed male mice, which is enhanced by a reduction in whole-body Slc2a2 expression. Mol Metab 77:101807.
121. Soták M, Casselbrant A, Rath E, et al. 2021. Intestinal sodium/glucose cotransporter 3 expression is epithelial and downregulated in obesity. Life Sci 267:118974.
122. Zhai Y, Liu X, Huang Z, et al. 2023. Data mining combines bioinformatics discover immunoinfiltration-related gene SERPINE1 as a biomarker for diagnosis and prognosis of stomach adenocarcinoma. Scientific reports 13:1373.
123. Liu Z, Chen X, Wang X, et al. 2011. Chemokine CXCL11 links microbial stimuli to intestinal inflammation. Clin Exp Immunol 164:396-406.
124. Kokkotis G, Filidou E, Tarapatzi G, et al. 2024. Oncostatin M Induces a Pro-inflammatory Phenotype in Intestinal Subepithelial Myofibroblasts. Inflammatory bowel diseases.
125. Glal D, Sudhakar JN, Lu HH, et al. 2018. ATF3 Sustains IL-22-Induced STAT3 Phosphorylation to Maintain Mucosal Immunity Through Inhibiting Phosphatases. Front Immunol 9:2522.
126. Cao Y, Yang Q, Deng H, et al. 2019. Transcriptional factor ATF3 protects against colitis by regulating follicular helper T cells in Peyer's patches. Proc Natl Acad Sci U S A 116:6286-6291.
127. Chapoval AI, Smithson G, Brunick L, et al. 2013. BTNL8, a butyrophilin-like molecule that costimulates the primary immune response. Mol Immunol 56:819-828.
128. Mayassi T, Ladell K, Gudjonson H, et al. 2019. Chronic Inflammation Permanently Reshapes Tissue-Resident Immunity in Celiac Disease. Cell 176:967-981.e919.

129. Rodriguez Sawicki L, Bottasso Arias NM, Scaglia N, et al. 2017. FABP1 knockdown in human enterocytes impairs proliferation and alters lipid metabolism. Biochim Biophys Acta Mol Cell Biol Lipids 1862:1587-1594.
130. Wang R, Kwon IK, Singh N, et al. 2014. Type 2 cGMP-dependent protein kinase regulates homeostasis by blocking c-Jun N-terminal kinase in the colon epithelium. Cell Death Differ 21:427-437.
131. Wang R, Islam BN, Bridges A, et al. 2017. cGMP Signaling Increases Antioxidant Gene Expression by Activating Forkhead Box O3A in the Colon Epithelium. Am J Pathol 187:377-389.
132. Tetteh PW, Kretzschmar K, Begthel H, et al. 2016. Generation of an inducible colon-specific Cre enzyme mouse line for colon cancer research. Proc Natl Acad Sci U S A 113:11859-11864.
133. Fukui H, Sekikawa A, Tanaka H, et al. 2011. DMBT1 is a novel gene induced by IL-22 in ulcerative colitis. Inflammatory bowel diseases 17:1177-1188.
134. Cayatte C, Joyce-Shaikh B, Vega F, et al. 2012. Biomarkers of Therapeutic Response in the IL-23 Pathway in Inflammatory Bowel Disease. Clin Transl Gastroenterol 3:e10.
135. Pulakazhi Venu VK, Alston L, Iftinca M, et al. 2021. Nr4A1 modulates inflammation-associated intestinal fibrosis and dampens fibrogenic signaling in myofibroblasts. Am J Physiol Gastrointest Liver Physiol 321:G280-g297.
136. Szczepanski HE, Flannigan KL, Mainoli B, et al. 2022. NR4A1 modulates intestinal smooth muscle cell phenotype and dampens inflammation-associated intestinal remodeling. Faseb j 36:e22609.
137. Sun EW, Martin AM, de Fontgalland D, et al. 2021. Evidence for Glucagon Secretion and Function Within the Human Gut. Endocrinology 162.
138. Krause WJ, Yamada J, Cutts JH. 1989. Enteroendocrine cells in the developing opossum small intestine and colon. J Anat 162:83-96.
139. Hoet RM, Voorsmit RA, Van Venrooij WJ. 1991. The perinuclear factor, a rheumatoid arthritis-specific autoantigen, is not present in keratohyalin granules of cultured buccal mucosa cells. Clin Exp Immunol 84:59-65.
140. Hughes CJ, Alderman C, Wolin AR, et al. 2024. All eyes on Eya: A unique transcriptional co-activator and phosphatase in cancer. Biochim Biophys Acta Rev Cancer 1879:189098.
141. Kriz V, Korinek V. 2018. Wnt, RSPO and Hippo Signalling in the Intestine and Intestinal Stem Cells. Genes (Basel) 9.
142. Li M, Zhang FJ, Bai RJ. 2024. The Hippo-YAP Signaling Pathway in Osteoarthritis and Rheumatoid Arthritis. J Inflamm Res 17:1105-1120.
143. Kim M, Jho EH. 2014. Cross-talk between Wnt/β-catenin and Hippo signaling pathways: a brief review. BMB reports 47:540-545.
144. Li XF, Yin SQ, Li H, et al. 2023. PPAR-γ alleviates the inflammatory response in TNF-α-induced fibroblast-like synoviocytes by binding to p53 in rheumatoid arthritis. Acta Pharmacol Sin 44:454-464.
145. Jüni P, Hari R, Rutjes AW, et al. 2015. Intra-articular corticosteroid for knee osteoarthritis. Cochrane Database Syst Rev 2015:Cd005328.
146. Reichenbach S, Rutjes AW, Nüesch E, et al. 2010. Joint lavage for osteoarthritis of the knee. Cochrane Database Syst Rev:Cd007320.
147. Xu L, Jiang H, Feng Y, et al. 2019. Peripheral and central substance P expression in rat CFA-induced TMJ synovitis pain. Mol Pain 15:1744806919866340.
148. Kaneguchi A, Ozawa J, Moriyama H, et al. 2017. Nociception contributes to the formation of myogenic contracture in the early phase of adjuvant-induced arthritis in a rat knee. J Orthop Res 35:1404-1413.
149. Bai Q, Cao J, Dong T, et al. 2020. Transcriptome Analysis of Dorsal Root Ganglion in Rats with Knee Joint Inflammation. J Pain Res 13:2709-2720.
150. Hallak M, Inal A, Baktir MA, et al. 2024. Comparison of disease-modifying anti-rheumatic drugs and hyperbaric oxygen therapy in the experimental model of rheumatoid arthritis in rats. Clin Exp Pharmacol Physiol 51:e13906.
151. Chen YF, Jobanputra P, Barton P, et al. 2006. A systematic review of the effectiveness of adalimumab, etanercept and infliximab for the treatment of rheumatoid arthritis in adults and an economic evaluation of their cost-effectiveness. Health Technol Assess 10:iii-iv, xi-xiii, 1-229.
152. Bordy R, Moretto J, Devaux S, et al. 2021. Adjuvant-induced arthritis is a relevant model to mimic coronary and myocardial impairments in rheumatoid arthritis. Joint Bone Spine 88:105069.

153. Vidal B, Cascão R, Finnilä MAJ, et al. 2018. Effects of tofacitinib in early arthritis-induced bone loss in an adjuvant-induced arthritis rat model. Rheumatology (Oxford) 57:1461-1471.
154. Robledo-González LE, Martínez-Martínez A, Vargas-Muñoz VM, et al. 2017. Repeated administration of mazindol reduces spontaneous pain-related behaviors without modifying bone density and microarchitecture in a mouse model of complete Freund's adjuvant-induced knee arthritis. J Pain Res 10:1777-1786.
155. Grandi FC, Modi H, Kampman L, et al. 2022. Chromatin accessibility profiling by ATAC-seq. Nat Protoc 17:1518-1552.
156. Agirman G, Yu KB, Hsiao EY. 2021. Signaling inflammation across the gut-brain axis. Science 374:1087-1092.
157. Holland AM, Bon-Frauches AC, Keszthelyi D, et al. 2021. The enteric nervous system in gastrointestinal disease etiology. Cell Mol Life Sci 78:4713-4733.
158. Chalazonitis A, Rao M. 2018. Enteric nervous system manifestations of neurodegenerative disease. Brain Res 1693:207-213.
159. Schneider KM, Blank N, Alvarez Y, et al. 2023. The enteric nervous system relays psychological stress to intestinal inflammation. Cell 186:2823-2838.e2820.
160. Guo H, Hu WC, Xian H, et al. 2024. CCL2 Potentiates Inflammation Pain and Related Anxiety-Like Behavior Through NMDA Signaling in Anterior Cingulate Cortex. Mol Neurobiol 61:4976-4991.
161. Wood JD. 2001. Enteric nervous system, serotonin, and the irritable bowel syndrome. Curr Opin Gastroenterol 17:91-97.
162. Liu MT, Rothstein JD, Gershon MD, et al. 1997. Glutamatergic enteric neurons. J Neurosci 17:4764-4784.
163. Boesmans W, Ameloot K, van den Abbeel V, et al. 2009. Cannabinoid receptor 1 signalling dampens activity and mitochondrial transport in networks of enteric neurones. Neurogastroenterol Motil 21:958-e977.
164. Liu DD, Lu JM, Zhao QR, et al. 2016. Growth differentiation factor-15 promotes glutamate release in medial prefrontal cortex of mice through upregulation of T-type calcium channels. Scientific reports 6:28653.
165. Vezyroglou A, Akilapa R, Barwick K, et al. 2022. The Phenotypic Continuum of ATP1A3-Related Disorders. Neurology 99:e1511-e1526.
166. Connor SA, Elegheert J, Xie Y, et al. 2019. Pumping the brakes: suppression of synapse development by MDGA-neuroligin interactions. Curr Opin Neurobiol 57:71-80.
167. Burclaff J, Bliton RJ, Breau KA, et al. 2022. A Proximal-to-Distal Survey of Healthy Adult Human Small Intestine and Colon Epithelium by Single-Cell Transcriptomics. Cell Mol Gastroenterol Hepatol 13:1554-1589.

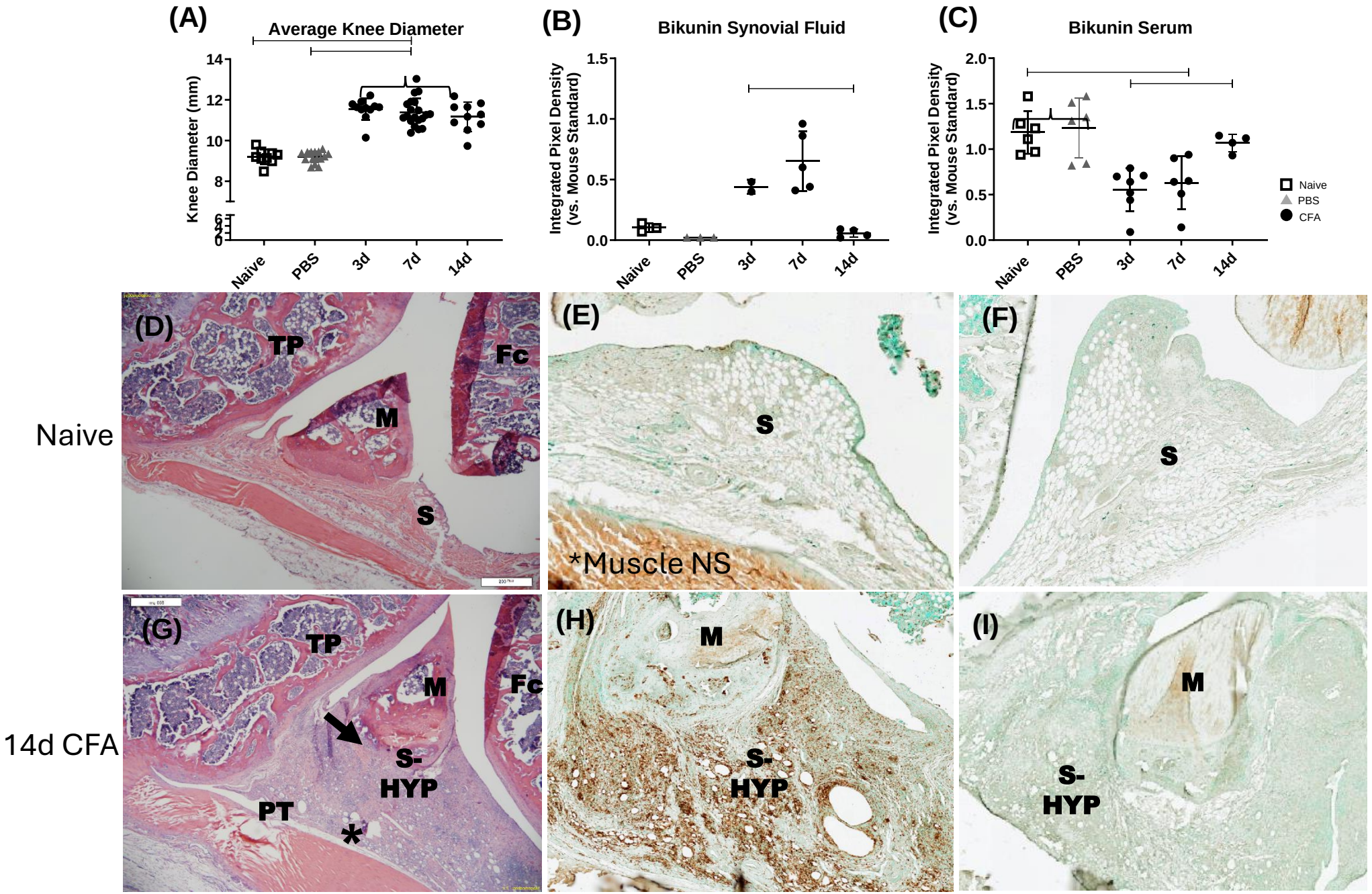
(A)
Average Knee Diameter
Knee Diameter (mm)
14
12
10
8
6
4
2
0
Naive
PBS
3d
7d
14d
(B)
Bikunin Synovial Fluid
Integrated Pixel Density (vs. Mouse Standard)
1.5
1.0
0.5
0.0
Naive
PBS
3d
7d
14d
(C)
Bikunin Serum
Integrated Pixel Density (vs. Mouse Standard)
2.0
1.5
1.0
0.5
0.0
Naive
PBS
3d
7d
14d
Naive
PBS
CFA
Naive
(D)
TP
Fc
M
S
(E)
S
*Muscle NS
(F)
S
14d CFA
(G)
TP
M
Fc
S-
HYP
PT
*
(H)
M
S-
HYP
(I)
M
S-
HYP

Fig. 1

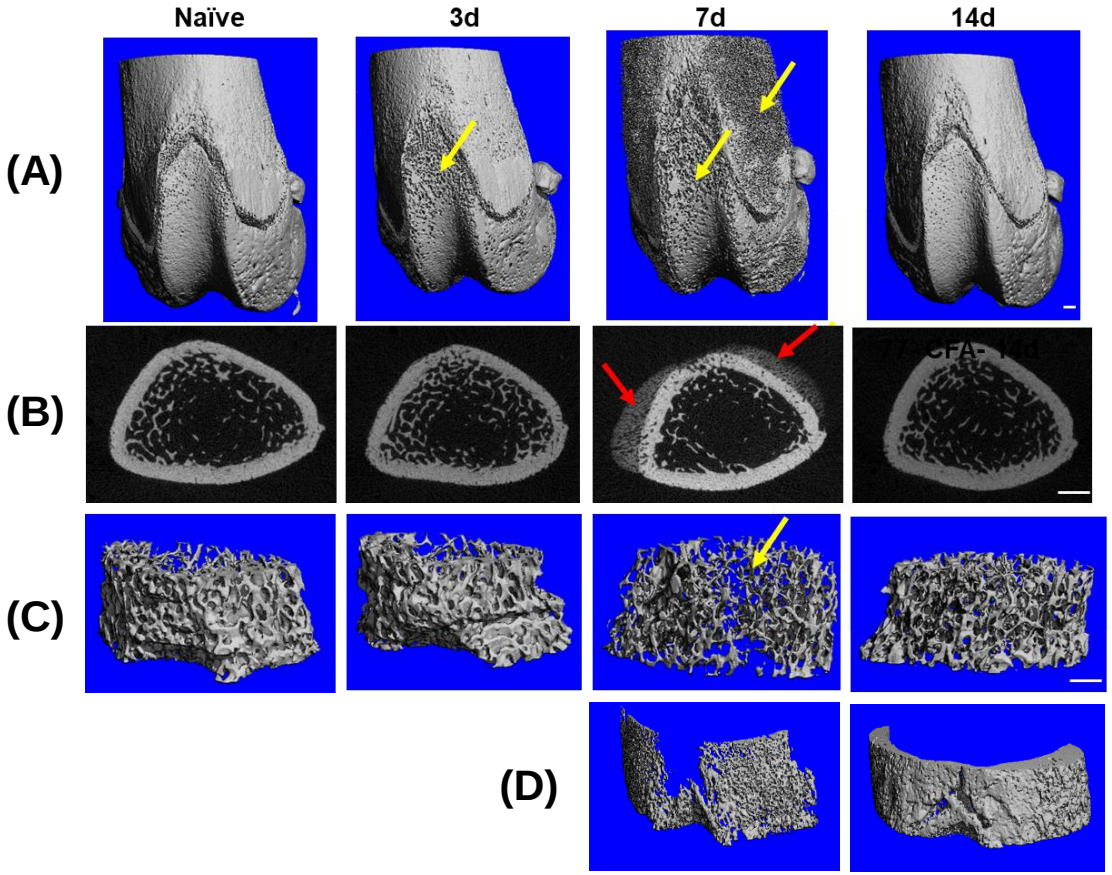
Naïve
3d
7d
14d
(A)
(B)
(C)
(D)

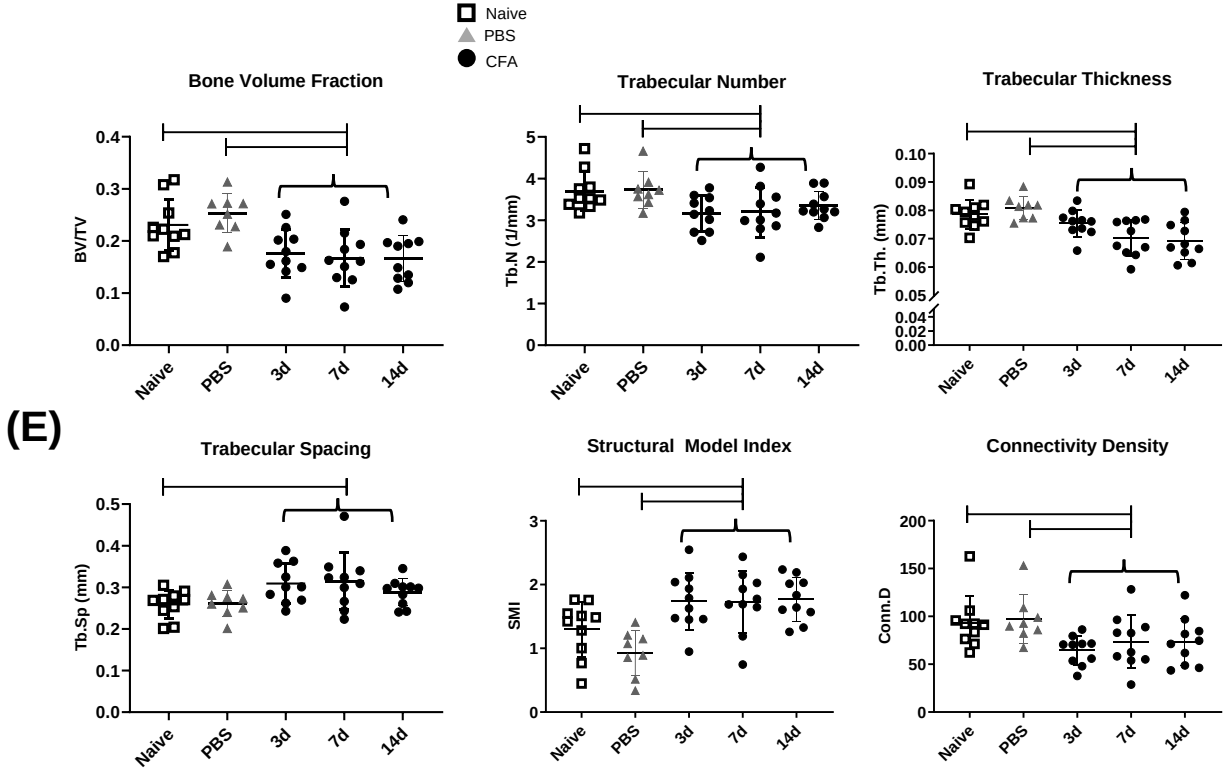
Naive
PBS
CFA
(E)
Bone Volume Fraction
BV/TV
Trabecular Number
Tb.N (1/mm)
Trabecular Thickness
Tb.Th. (mm)
Trabecular Spacing
Tb.Sp (mm)
Structural Model Index
SMI
Connectivity Density
Conn.D
Naive
PBS
3d
7d
14d

Fig. 2

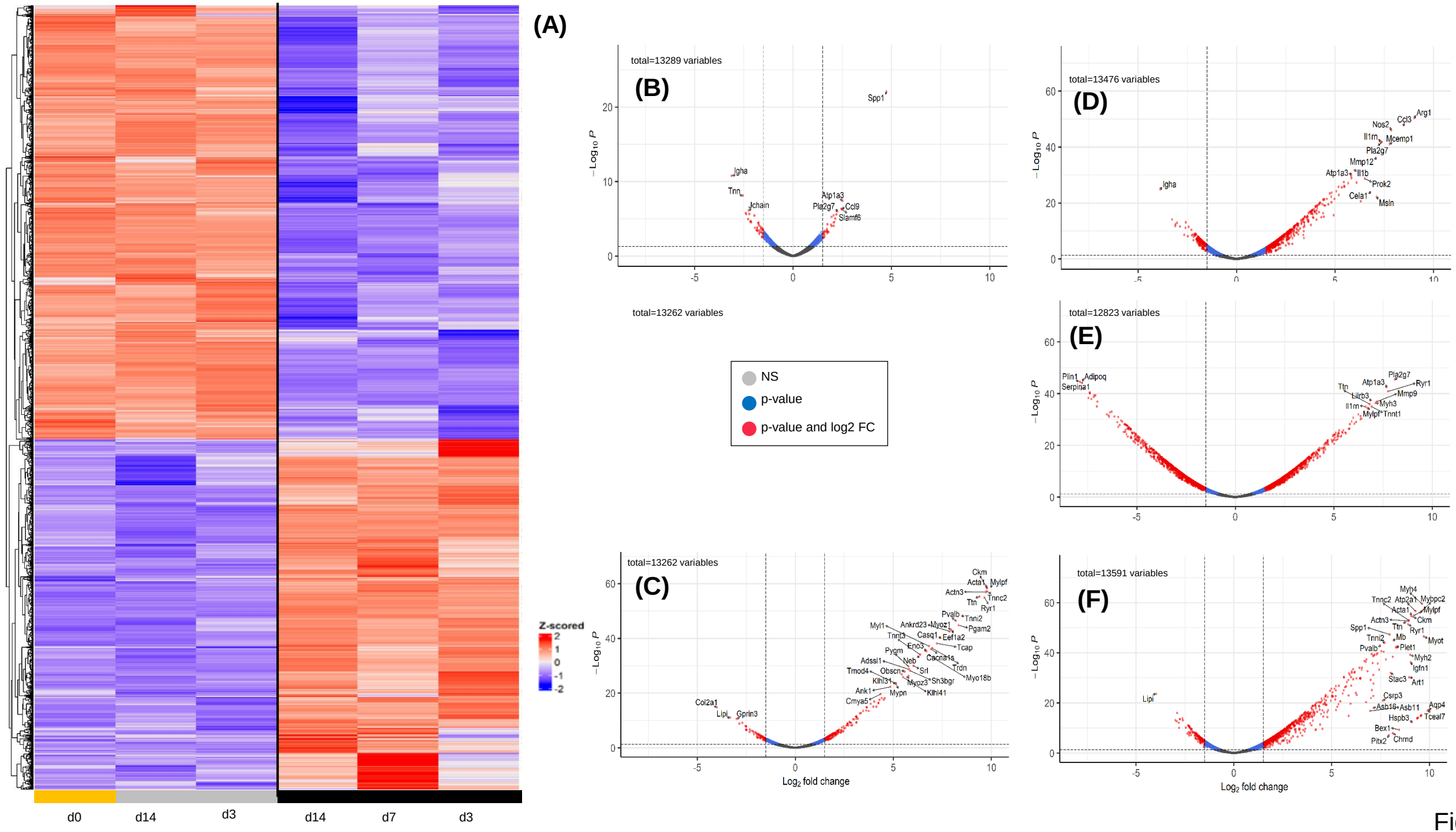
(A)
d0
d14
d3
d14
d7
d3
Z-scored
2
1
0
-1
-2
(B)
total=13289 variables
Spp1
Igha
Tnn
Jchain
Atp1a3
Pla2g7
Ccl9
Slamf6
(C)
total=13262 variables
Ckm
Acta1
Mylpf
Actn3
Tnnc2
Ttn
Ryr1
Pvalb
Tnni2
Pgam2
Myl1
Ankrd23
Myoz1
Tnnt3
Casq1
Eef1a2
Tcap
Pygm
Eno3
Cacna1s
Adssl1
Neb
Trdn
Tmod4
Obscn
Srl
Myo18b
Klhl31
Myoz3
Sh3bgr
Ank1
Mypn
Klhl41
Cmya5
Col2a1
Lipi
Gprin3
(D)
total=13476 variables
Nos2
Ccl3
Arg1
Il1rn
Mcemp1
Pla2g7
Mmp12
Atp1a3
Il1b
Prok2
Igha
Cela1
Msln
(E)
total=12823 variables
Plin1
Adipoq
Serpina1
Pla2g7
Atp1a3
Ryr1
Ttn
Mmp9
Lilrb3
Myh3
Il1rn
Mylpf
Tnnt1
(F)
total=13591 variables
Myh4
Tnnc2
Atp2a1
Mybpc2
Acta1
Mylpf
Actn3
Ckm
Ttn
Spp1
Ryr1
Tnni2
Mb
Myot
Pvalb
Plet1
Myh2
Igfn1
Stac3
Art1
Lipi
Csrp3
Asb16
Asb11
Aqp4
Hspb3
Tceal7
Bex1
Pitx2
Chrmd
total=13262 variables
NS
p-value
p-value and log2 FC
$-\mathrm{Log}_{10}\,P$
Log_2 fold change

Fig 3

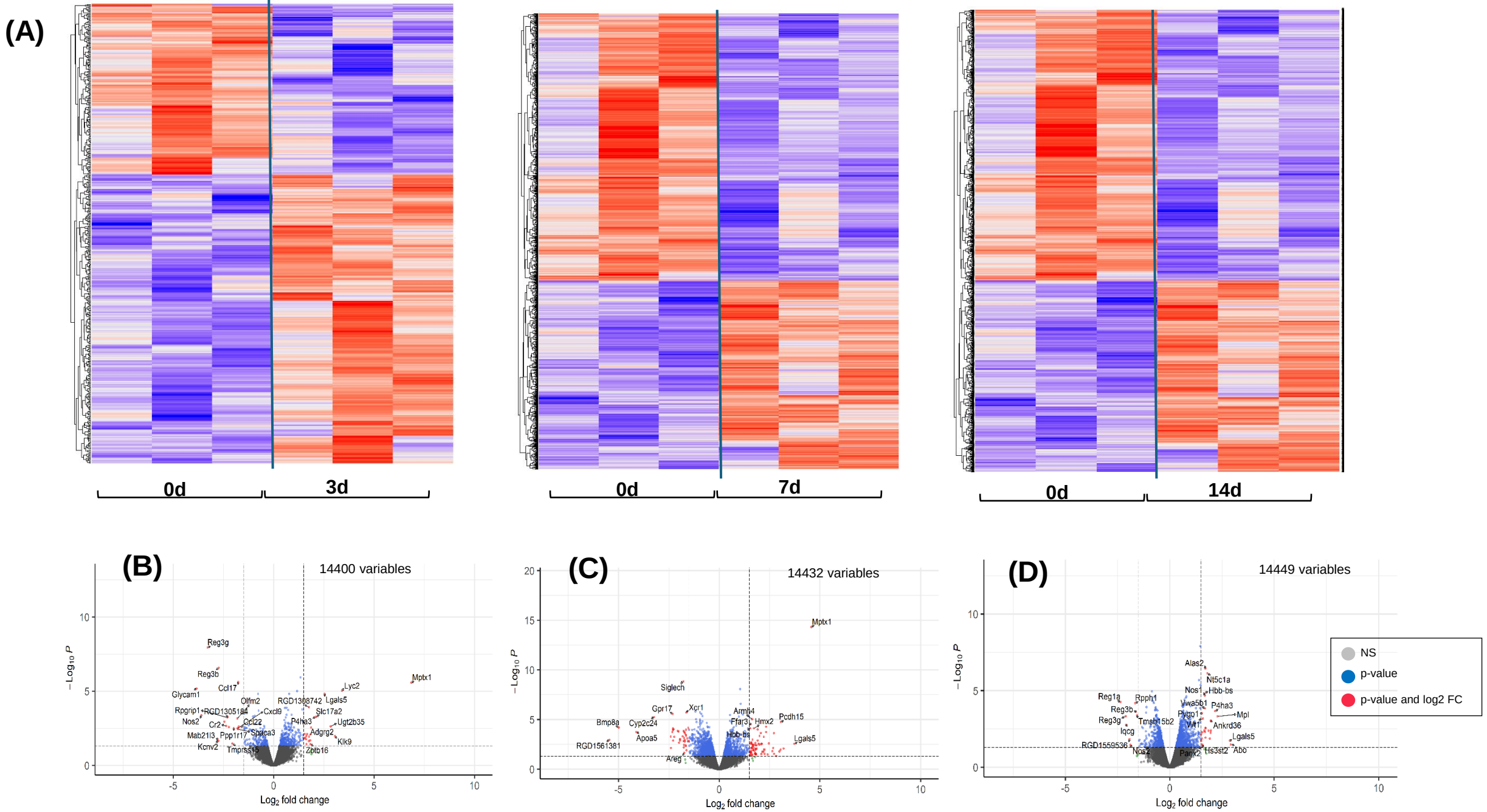
(A)
0d
3d
0d
7d
0d
14d
(B)
14400 variables
Reg3g
Reg3b
Ccl17
Glycam1
Olfm2
RGD1308742
Lgals5
Lyc2
Mptx1
Rpgrip1
RGD1305184
Cxcl9
Slc17a2
Nos2
Cr2
Ccl22
P4ha3
Ugt2b35
Mab21l3
Ppp1r17
Spaca3
Adgrg2
Klk9
Kcnv2
Tmprss13
Zbtb16
$-\mathrm{Log}_{10}\,P$
Log_2 fold change
(C)
14432 variables
Mptx1
Siglech
Gpr17
Xcr1
Armh4
Pcdh15
Bmp8a
Cyp2c24
Ffar3
Hmx2
Apoa5
Hbb-bs
Lgals5
RGD1561381
Areg
$-\mathrm{Log}_{10}\,P$
Log_2 fold change
(D)
14449 variables
Alas2
Nt5c1a
Nos1
Hbb-bs
Reg1a
Rpph1
Vwa5b1
P4ha3
Reg3b
Pygo1
Mpl
Reg3g
Tmsb15b2
Wt1
Ankrd36
Iqcg
Lgals5
RGD1559536
Nos2
Panx2
Hs3st2
Abo
NS
p-value
p-value and log2 FC
$-\mathrm{Log}_{10}\,P$
Log_2 fold change

Fig 4

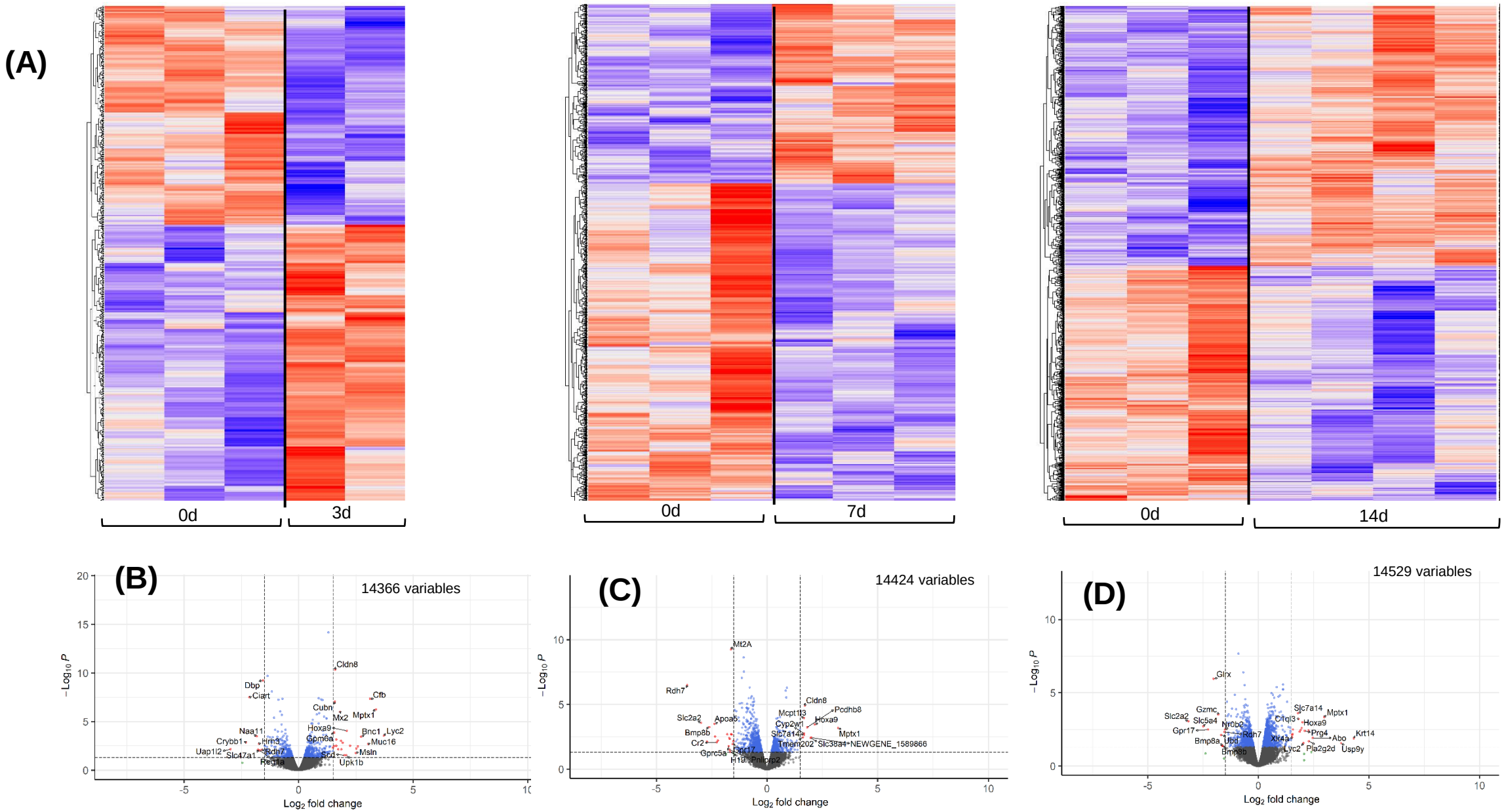
(A)
0d
3d
0d
7d
0d
14d
(B)
14366 variables
Cldn8
Dbp
Ciart
Cfb
Cubn
Mx2
Mptx1
Hoxa9
Naa11
Bnc1
Lyc2
Crybb1
Hrn3
Gpm6a
Muc16
Uap1l2
Rdh7
Msln
Slc47a1
Scd
Reg1a
Upk1b
−Log10 P
Log2 fold change
(C)
14424 variables
Mt2A
Rdh7
Cldn8
Pcdhb8
Slc2a2
Apoa5
Mcpt1l3
Hoxa9
Cyp2w1
Bmp8b
Slc7a14
Mptx1
Cr2
Tmem202
Slc38a4
NEWGENE_1589866
Gprc5a
Gpr17
H19
Pnlprp2
−Log10 P
Log2 fold change
(D)
14529 variables
Glrx
Gzmc
Slc7a14
Mptx1
Slc2a2
Slc5a4
C1ql3
Hoxa9
Nr0b2
Gpr17
Rdh7
Prg4
Abo
Krt14
Bmp8a
Ubd
Xlr4a
Lyc2
Pla2g2d
Usp9y
Bmp8b
−Log10 P
Log2 fold change

Fig 5

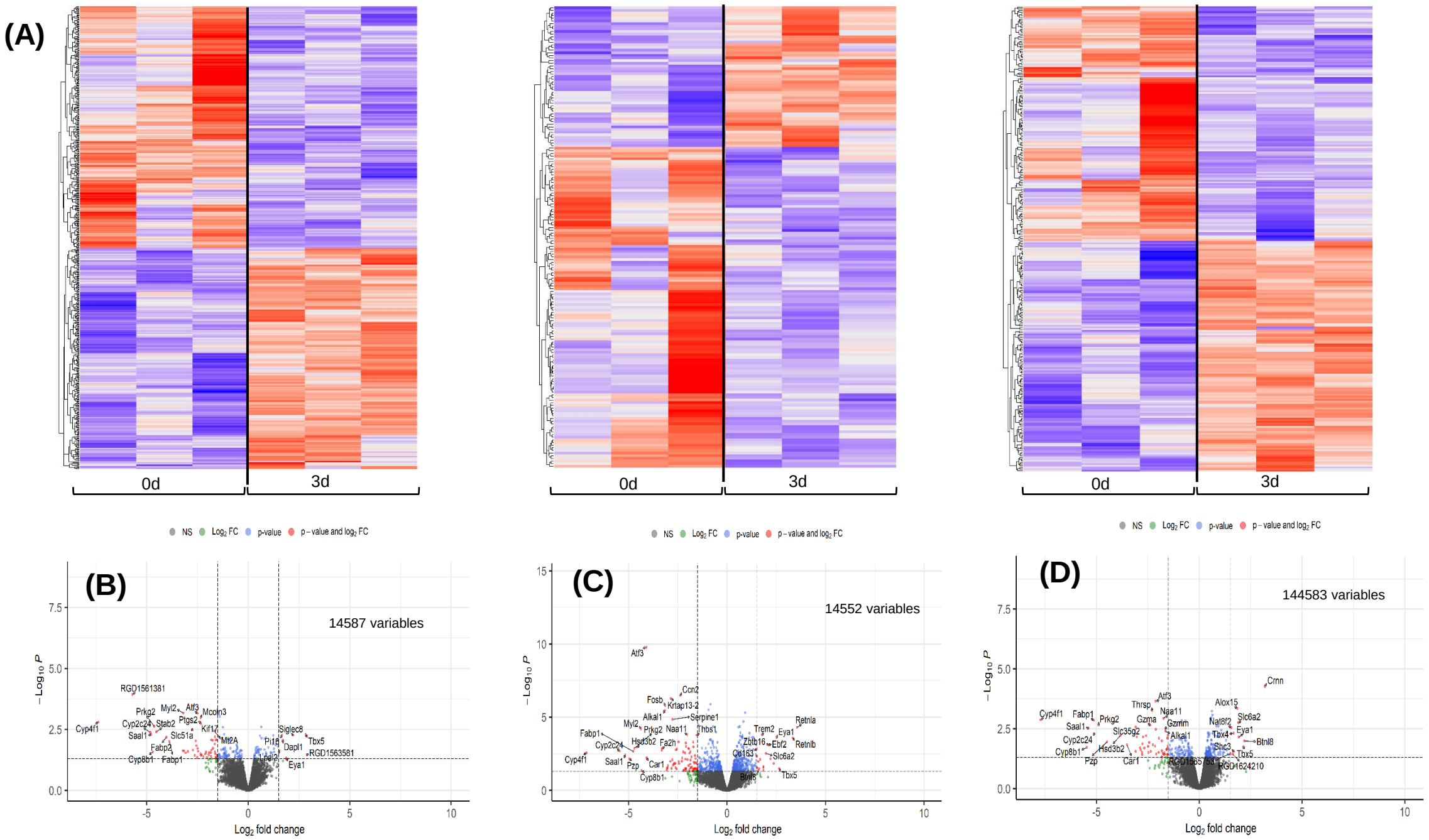
(A)
0d
3d
NS
Log2 FC
p-value
p – value and log2 FC
(B)
14587 variables
RGD1561381
Prkg2
Myl2
Atf3
Mcoln3
Cyp2c24
Stab2
Ptgs2
Kif17
Cyp4f1
Saal1
Slc51a
Mt2A
Fabp2
Cyp8b1
Fabp1
Pi16
Siglec8
Dapl1
Tbx5
RGD1563581
Eya1
Log2 fold change
−Log10 P
(C)
14552 variables
Atf3
Ccn2
Fosb
Krtap13-2
Alkal1
Serpine1
Myl2
Prkg2
Naa11
Thbs1
Fabp1
Cyp2c24
Hsd3b2
Fa2h
Cyp4f1
Saal1
Pzp
Car1
Cyp8b1
Trem2
Eya1
Retnla
Zbtb16
Ebf2
Retnlb
Cd163
Slc6a2
Btnl8
Tbx5
(D)
144583 variables
Crnn
Atf3
Thrsp
Naa11
Alox15
Cyp4f1
Fabp1
Prkg2
Gzma
Gzmm
Nat8f2
Slc6a2
Saal1
Slc35g2
Alkal1
Tbx4
Eya1
Cyp2c24
Hsd3b2
Shc3
Btnl8
Cyp8b1
Tbx5
Pzp
Car1
RGD1565753
RGD1624210

Fig 6

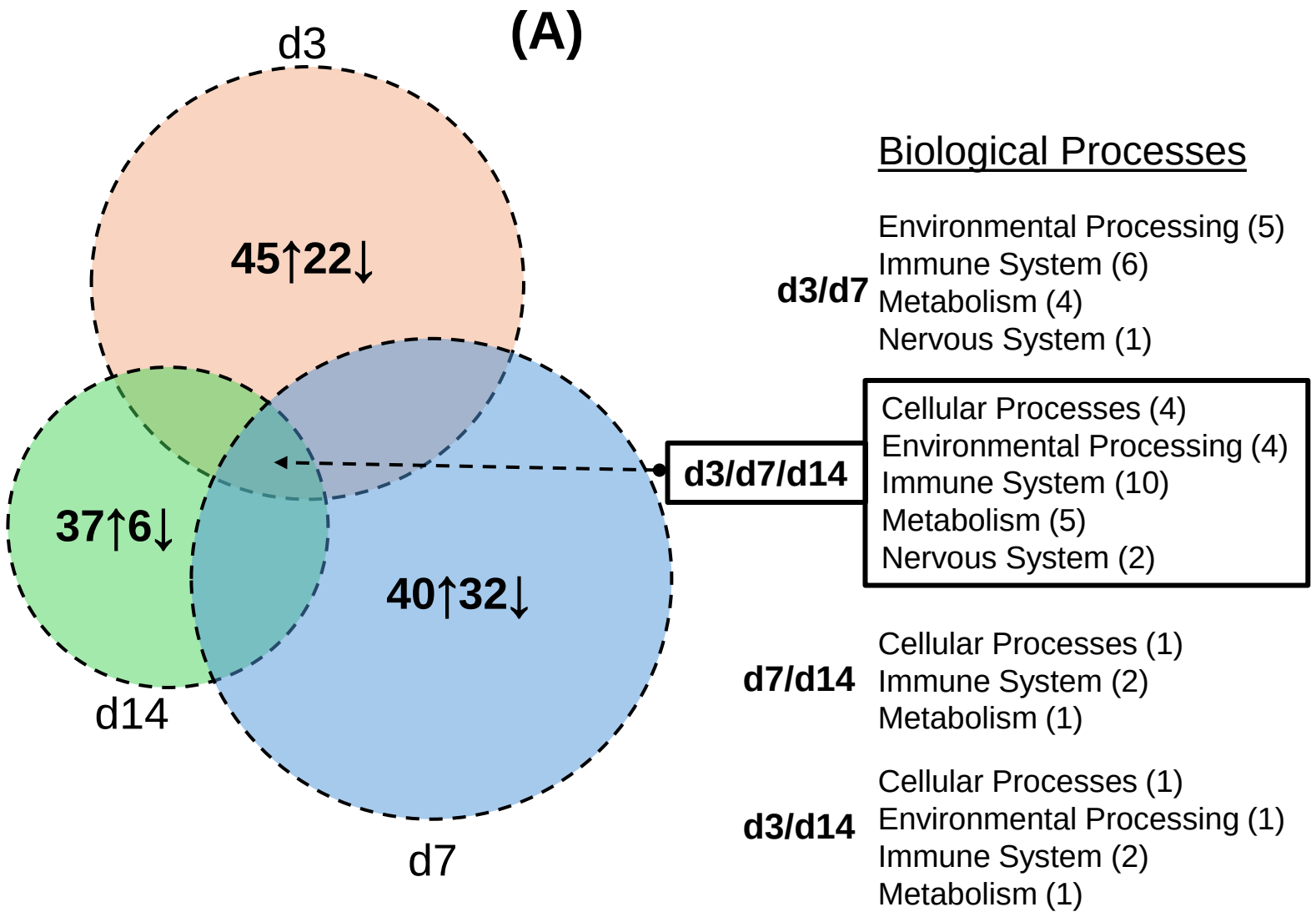
(A)
d3
45↑22↓
37↑6↓
40↑32↓
d14
d7
Biological Processes
d3/d7
Environmental Processing (5)
Immune System (6)
Metabolism (4)
Nervous System (1)
d3/d7/d14
Cellular Processes (4)
Environmental Processing (4)
Immune System (10)
Metabolism (5)
Nervous System (2)
d7/d14
Cellular Processes (1)
Immune System (2)
Metabolism (1)
d3/d14
Cellular Processes (1)
Environmental Processing (1)
Immune System (2)
Metabolism (1)

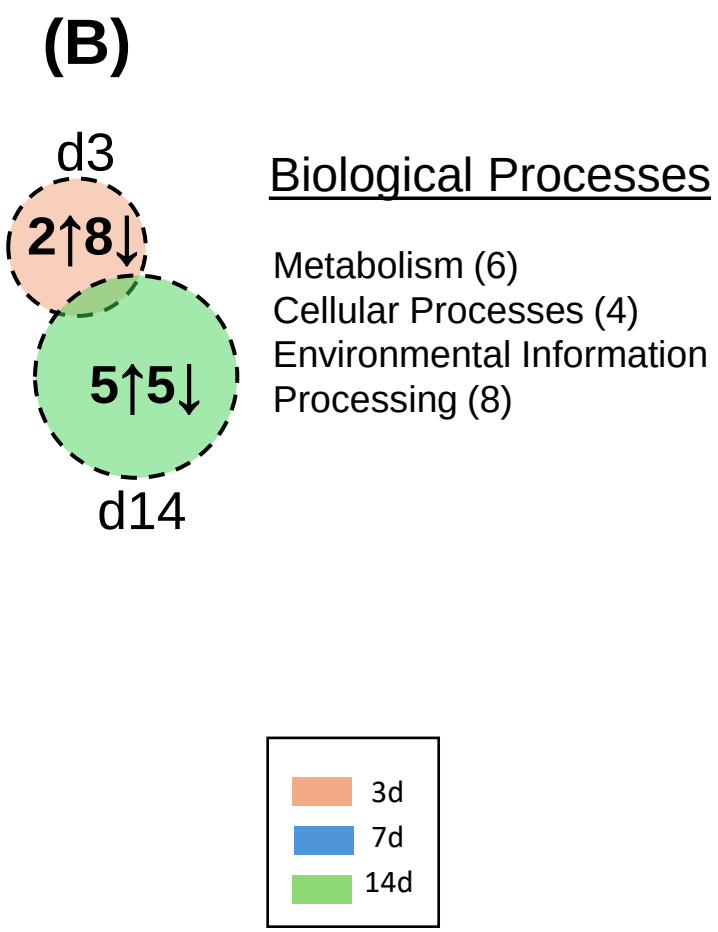
(B)
d3
2↑8↓
5↑5↓
d14
Biological Processes
Metabolism (6)
Cellular Processes (4)
Environmental Information Processing (8)
3d
7d
14d

Fig 7

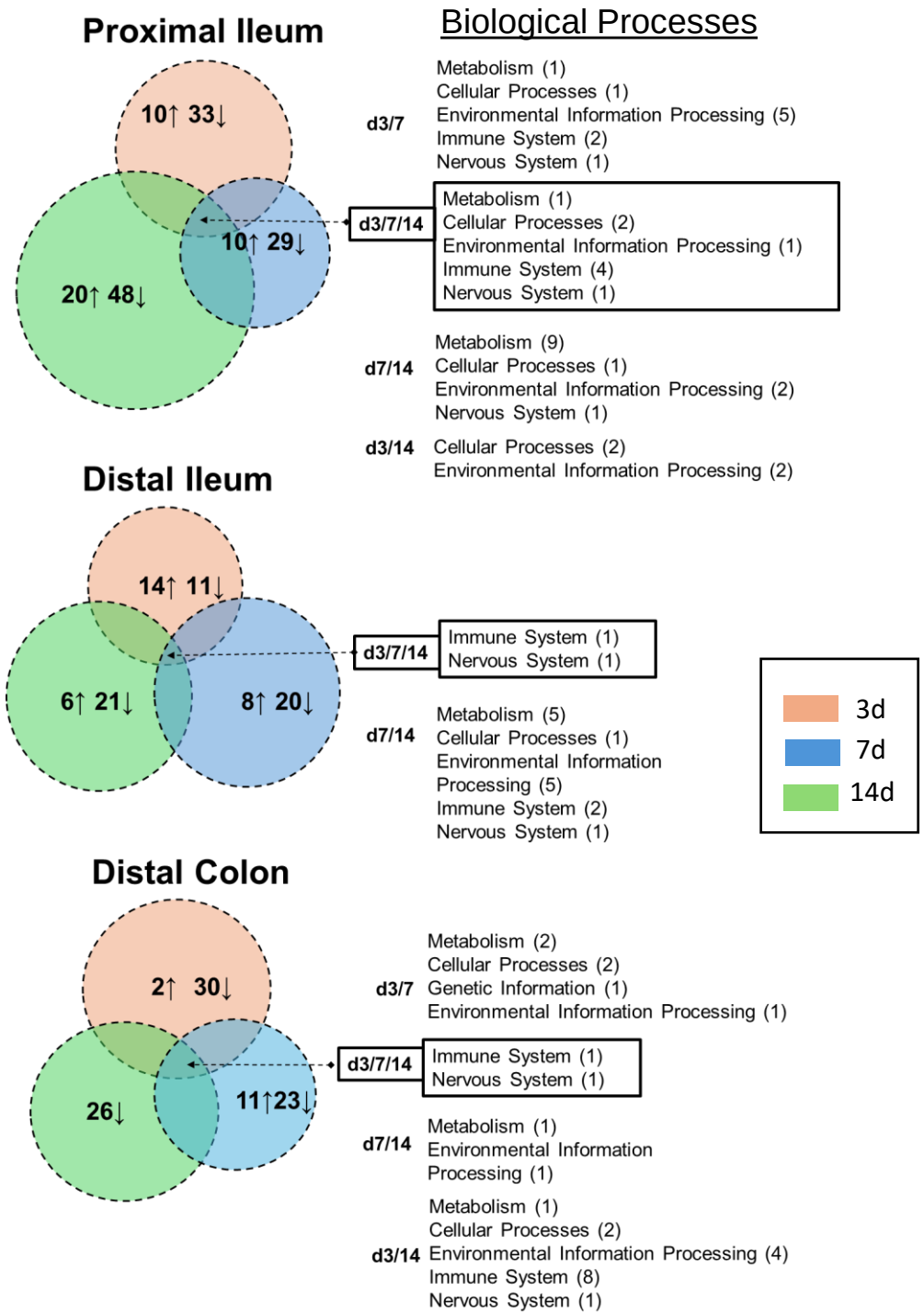
Biological Processes
Proximal Ileum
10↑ 33↓
10↑ 29↓
20↑ 48↓
d3/7
Metabolism (1)
Cellular Processes (1)
Environmental Information Processing (5)
Immune System (2)
Nervous System (1)
d3/7/14
Metabolism (1)
Cellular Processes (2)
Environmental Information Processing (1)
Immune System (4)
Nervous System (1)
d7/14
Metabolism (9)
Cellular Processes (1)
Environmental Information Processing (2)
Nervous System (1)
d3/14
Cellular Processes (2)
Environmental Information Processing (2)
Distal Ileum
14↑ 11↓
6↑ 21↓
8↑ 20↓
d3/7/14
Immune System (1)
Nervous System (1)
d7/14
Metabolism (5)
Cellular Processes (1)
Environmental Information Processing (5)
Immune System (2)
Nervous System (1)
3d
7d
14d
Distal Colon
2↑ 30↓
26↓
11↑23↓
d3/7
Metabolism (2)
Cellular Processes (2)
Genetic Information (1)
Environmental Information Processing (1)
d3/7/14
Immune System (1)
Nervous System (1)
d7/14
Metabolism (1)
Environmental Information Processing (1)
d3/14
Metabolism (1)
Cellular Processes (2)
Environmental Information Processing (4)
Immune System (8)
Nervous System (1)

Fig 8

Environmental Information Processing	Chemokine signaling	↑	↓	↓	↓	Chemokine signaling	↑	↔	↓	↓	Chemokine signaling	↑	↓	↓	↔
	Cytokine−cytokine receptor interaction	↑	↔	↔	↓	Cytokine−cytokine receptor interaction	↑	↓	↓	↓	Cytokine−cytokine receptor interaction	↑	↔	↓	↓
	IL−17 signaling	↑	↓	↔	↔	IL−17 signaling	↑	↔	↔	↔	IL−17 signaling	↑	↔	↔	↓
	JAK−STAT signaling	↑	↓	↔	↔	JAK−STAT signaling	↔	↓	↓	↓	JAK−STAT signaling	↔	↔	↔	↔
	NF−kappa B signaling	↑	↔	↔	↓	NF−kappa B signaling	↑	↔	↔	↓	NF−kappa B signaling	↑	↔	↔	↔
	TNF signaling	↑	↓	↓	↔	TNF signaling	↔	↔	↓	↔	TNF signaling	↑	↓	↓	↔
	PPAR signaling pathway	↓	↓	↓	↓	PPAR signaling pathway	↓	↓	↓	↓	PPAR signaling pathway	↓	↓	↓	↓
Immune System	Antigen processing and presentation	↔	↓	↔	↓	Antigen processing and presentation	↑	↓	↓	↓	Antigen processing and presentation	↑	↓	↓	↔
	B cell receptor signaling	↔	↓	↔	↓	B cell receptor signaling	↑	↔	↓	↓	B cell receptor signaling	↑	↓	↔	↔
	C−type lectin receptor signaling	↑	↓	↔	↓	C−type lectin receptor signaling	↑	↔	↓	↓	C−type lectin receptor signaling	↑	↔	↔	↔
	Apoptosis	↔	↔	↔	↔	Apoptosis	↑	↓	↓	↓	Apoptosis	↑	↓	↓	↔
	Efferocytosis	↑	↓	↔	↔	Efferocytosis	↑	↔	↓	↔	Efferocytosis	↔	↔	↓	↔
	Lysosome	↑	↔	↔	↔	Lysosome	↑	↓	↔	↔	Lysosome	↑	↓	↓	↔
	Necroptosis	↑	↓	↔	↔	Necroptosis	↑	↓	↓	↔	Necroptosis	↑	↓	↓	↔
	NK cell mediated cytotoxicity	↔	↓	↔	↔	NK cell mediated cytotoxicity	↑	↓	↓	↓	NK cell mediated cytotoxicity	↑	↔	↓	↔
	NOD−like receptor signaling	↑	↓	↔	↔	NOD−like receptor signaling	↑	↔	↔	↓	NOD−like receptor signaling	↔	↓	↓	↓
	Phagosome	↑	↓	↔	↓	Phagosome	↑	↓	↓	↓	Phagosome	↑	↓	↓	↔
	T cell receptor signaling	↔	↓	↔	↓	T cell receptor signaling	↑	↔	↓	↓	T cell receptor signaling	↑	↓	↓	↔
	Th1 and Th2 cell differentiation	↔	↓	↓	↓	Th1 and Th2 cell differentiation	↑	↓	↓	↓	Th1 and Th2 cell differentiation	↑	↓	↓	↔
	Th17 cell differentiation	↔	↓	↔	↓	Th17 cell differentiation	↑	↓	↓	↓	Th17 cell differentiation	↑	↓	↓	↔
	Toll−like receptor signaling	↑	↓	↔	↔	Toll−like receptor signaling	↑	↓	↓	↓	Toll−like receptor signaling	↑	↓	↓	↔
Metabolism	Oxidative phosphorylation	↑	↓	↓	↓	Oxidative phosphorylation	↑	↓	↓	↓	Oxidative phosphorylation	↑	↓	↓	↓

Fig 9

(A)

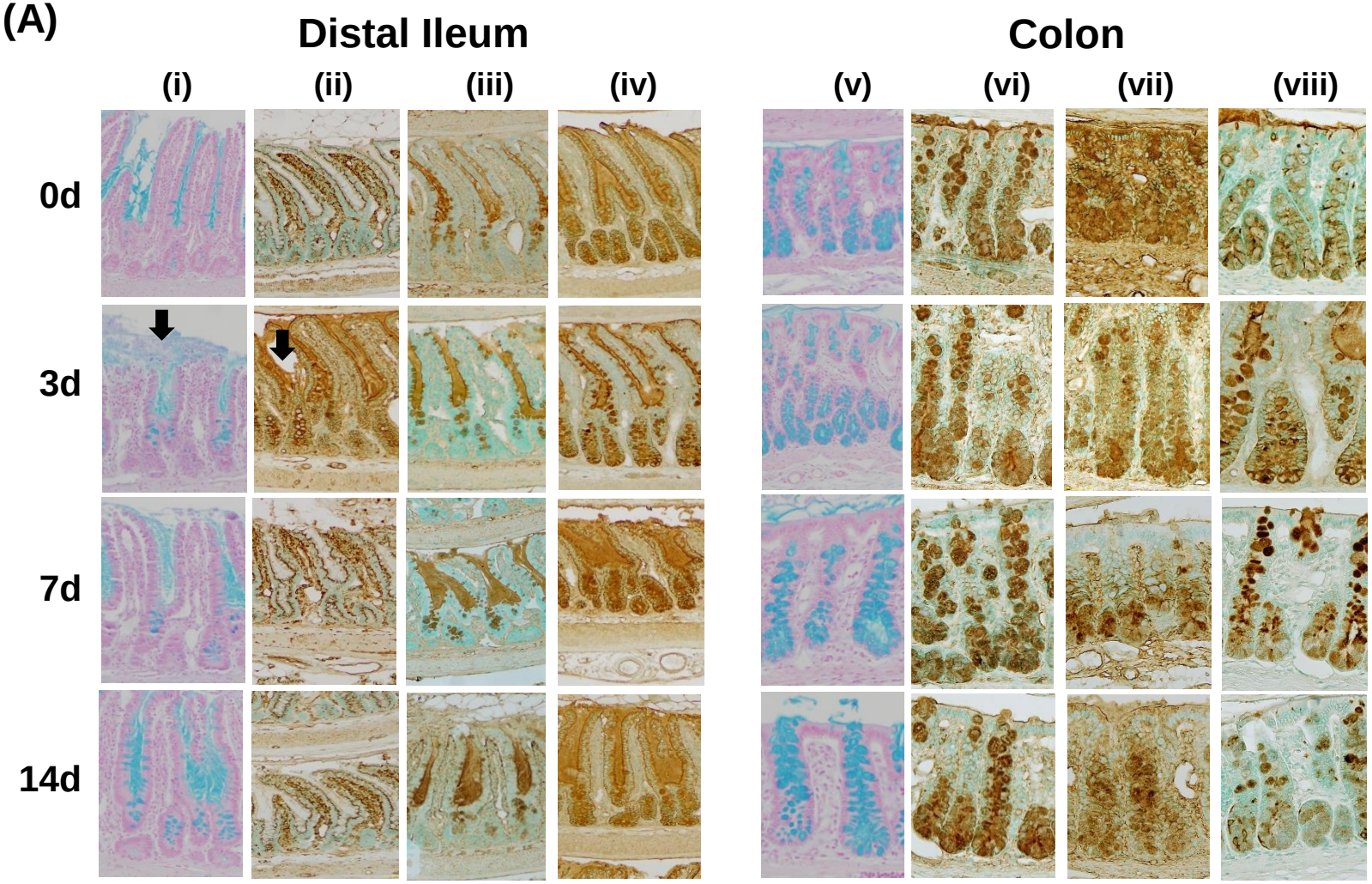
Distal Ileum
Colon
(i)
(ii)
(iii)
(iv)
(v)
(vi)
(vii)
(viii)
0d
3d
7d
14d

(B)

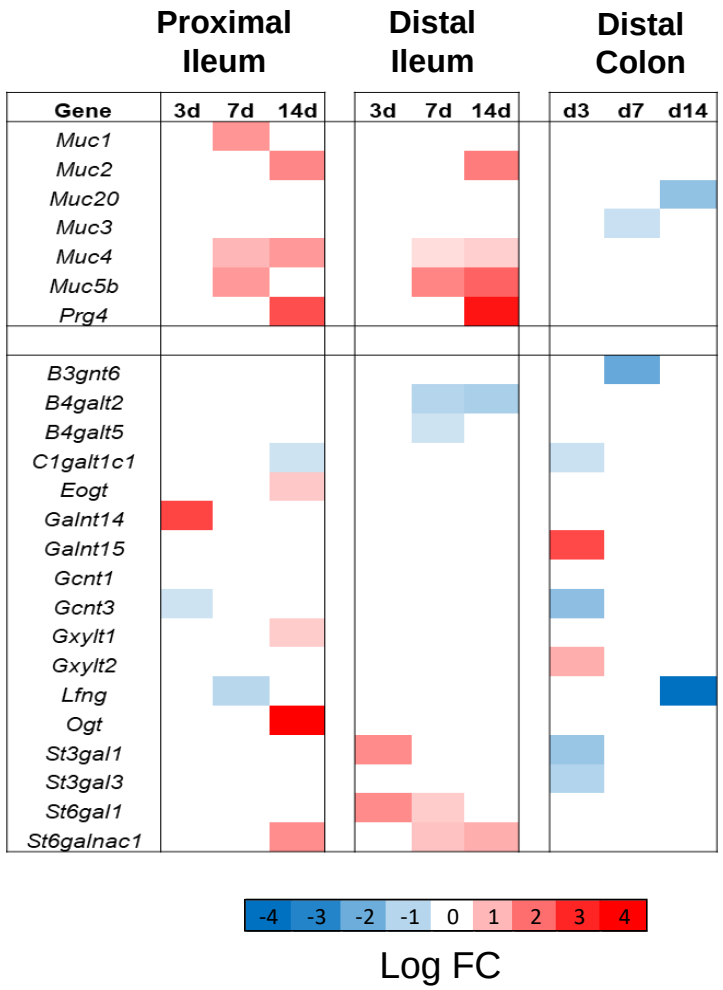
Proximal Ileum
Distal Ileum
Distal Colon
Gene
3d
7d
14d
3d
7d
14d
d3
d7
d14
Muc1
Muc2
Muc20
Muc3
Muc4
Muc5b
Prg4
B3gnt6
B4galt2
B4galt5
C1galt1c1
Eogt
Galnt14
Galnt15
Gcnt1
Gcnt3
Gxylt1
Gxylt2
Lfng
Ogt
St3gal1
St3gal3
St6gal1
St6galnac1
-4
-3
-2
-1
0
1
2
3
4
Log FC

Fig 10

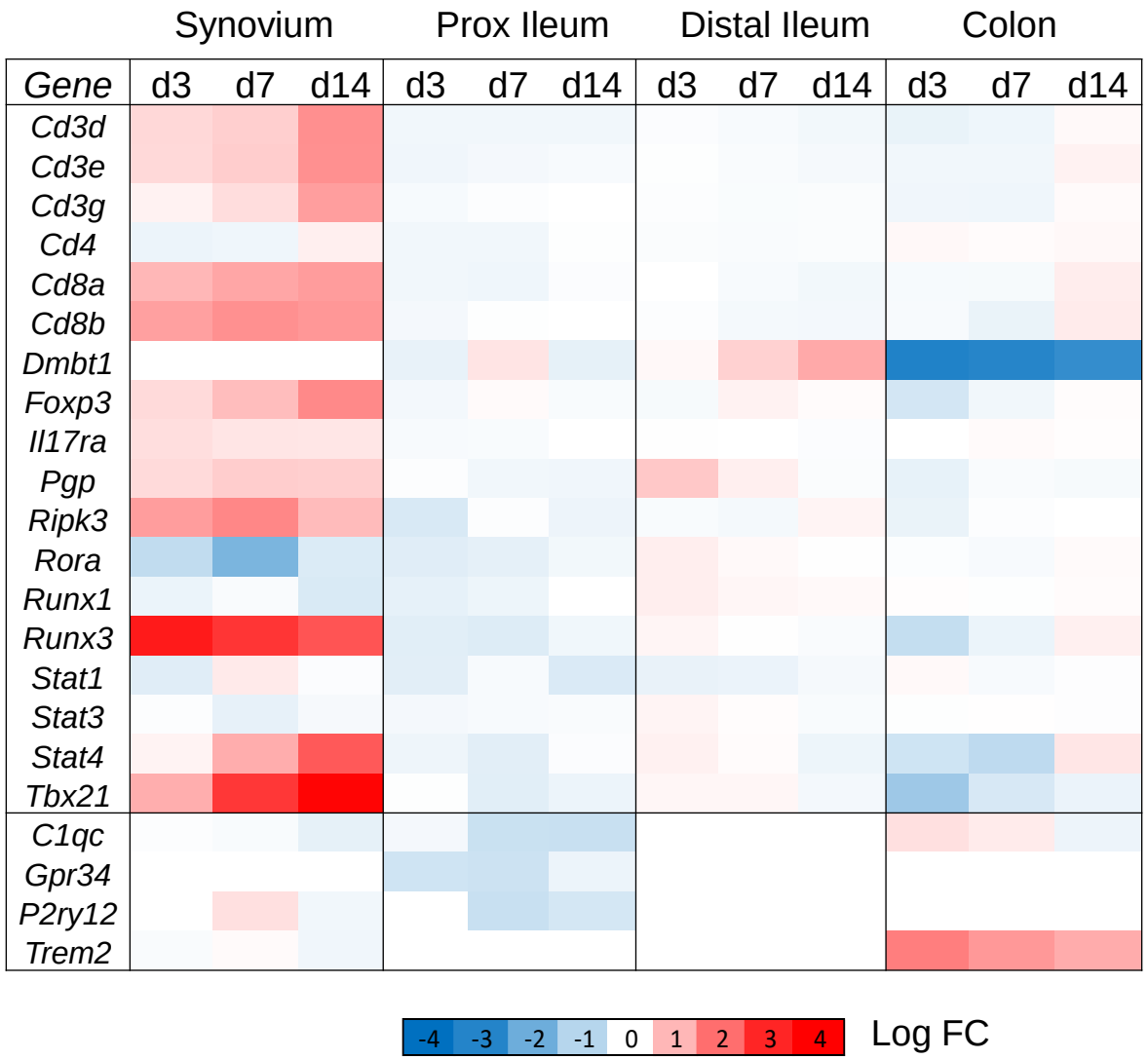
Synovium
Prox Ileum
Distal Ileum
Colon
Gene
d3
d7
d14
d3
d7
d14
d3
d7
d14
d3
d7
d14
Cd3d
Cd3e
Cd3g
Cd4
Cd8a
Cd8b
Dmbt1
Foxp3
Il17ra
Pgp
Ripk3
Rora
Runx1
Runx3
Stat1
Stat3
Stat4
Tbx21
C1qc
Gpr34
P2ry12
Trem2
-4
-3
-2
-1
0
1
2
3
4
Log FC

Fig 11

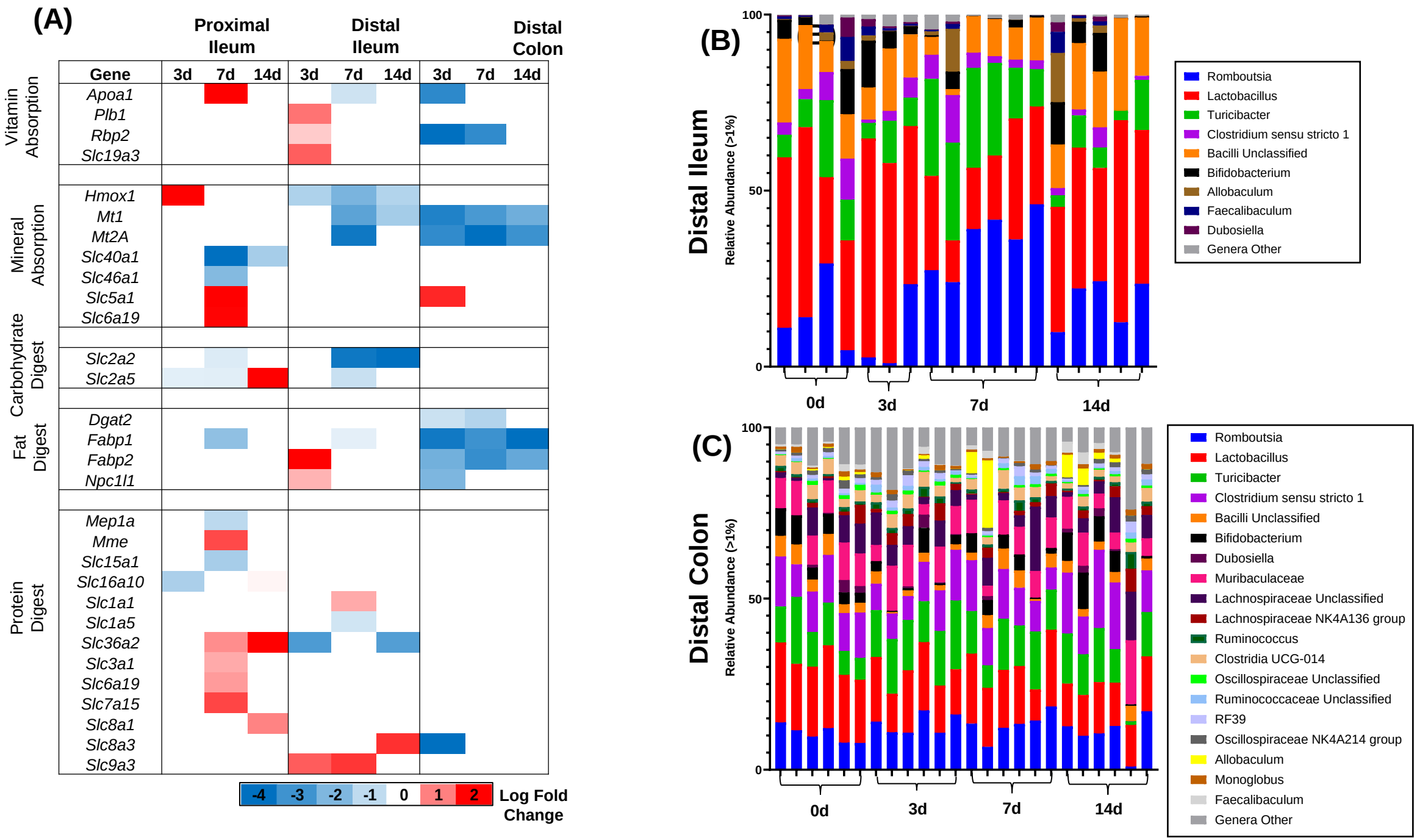
(A)
Proximal Ileum
Distal Ileum
Distal Colon
Gene
3d
7d
14d
Vitamin Absorption
Apoa1
Plb1
Rbp2
Slc19a3
Mineral Absorption
Hmox1
Mt1
Mt2A
Slc40a1
Slc46a1
Slc5a1
Slc6a19
Carbohydrate Digest
Slc2a2
Slc2a5
Fat Digest
Dgat2
Fabp1
Fabp2
Npc1l1
Protein Digest
Mep1a
Mme
Slc15a1
Slc16a10
Slc1a1
Slc1a5
Slc36a2
Slc3a1
Slc6a19
Slc7a15
Slc8a1
Slc8a3
Slc9a3
-4
-3
-2
-1
0
1
2
Log Fold Change
(B)
Distal Ileum
Relative Abundance (>1%)
100
50
0
0d
3d
7d
14d
Romboutsia
Lactobacillus
Turicibacter
Clostridium sensu stricto 1
Bacilli Unclassified
Bifidobacterium
Allobaculum
Faecalibaculum
Dubosiella
Genera Other
(C)
Distal Colon
Relative Abundance (>1%)
100
50
0
0d
3d
7d
14d
Romboutsia
Lactobacillus
Turicibacter
Clostridium sensu stricto 1
Bacilli Unclassified
Bifidobacterium
Dubosiella
Muribaculaceae
Lachnospiraceae Unclassified
Lachnospiraceae NK4A136 group
Ruminococcus
Clostridia UCG-014
Oscillospiraceae Unclassified
Ruminococcaceae Unclassified
RF39
Oscillospiraceae NK4A214 group
Allobaculum
Monoglobus
Faecalibaculum
Genera Other

Fig 12